Transcriptional profiling reveals TRPM5-expressing cells involved in viral infection in the olfactory epithelium

B. Dnate' Baxter[1,2,‡], Eric D. Larson[3 ‡], Paul Feinstein[4], Arianna Gentile Polese[1,2], Andrew N. Bubak[5], Christy S. Niemeyer[5], James Hassell, Jr.[5], Laetitia Merle[1,2], Doug Shepherd[6], Vijay R. Ramakrishnan[3], Maria A. Nagel[5], and Diego Restrepo[1,2,*]

[1]Neuroscience Graduate Program, University of Colorado Anschutz Medical Campus, Aurora, CO 80045, USA

[2]Department of Cell and Developmental Biology, University of Colorado Anschutz Medical Campus, Aurora, CO 80045, USA

[3]Department of Otolaryngology, University of Colorado Anschutz Medical Campus, Aurora, CO 80045, USA

[4]Department of Biological Sciences, Hunter College, CUNY, New York, NY, 10065, USA

[5]Department of Neurology, University of Colorado Anschutz Medical Campus, Aurora, CO 80045, USA

[6]Department of Pharmacology, University of Colorado Anschutz Medical Campus and Center for Biological Physics and Department of Physics, Arizona State University, USA

[‡]Co-first authors

[*]Corresponding author: Diego Restrepo, diego.restrepo@cuanschutz.edu

Abstract

Background: Understanding viral infection of the olfactory epithelium is essential because smell loss can occur with coronavirus disease 2019 (COVID-19), caused by severe acute respiratory syndrome coronavirus clade 2 (SARS-CoV-2), and because the olfactory nerve is an important route of entry for viruses to the central nervous system. Specialized chemosensory epithelial cells that express the transient receptor potential cation channel subfamily M member 5 (TRPM5) are found throughout the airways and intestinal epithelium and are involved in responses to viral infection.

Results: Herein we performed deep transcriptional profiling of olfactory epithelial cells sorted by flow cytometry based on the expression of fluorescent protein markers for olfactory sensory neurons and TRPM5 in the mouse (*Mus musculus*). We find profuse expression of transcripts involved in inflammation, immunity and viral infection in TRPM5-expressing microvillous cells and olfactory sensory neurons. These cells express the *Tmprss2* transcript that encodes for a serine protease that primes the SARS-CoV-2 spike protein before entry into host cells. Intranasal infection with herpes simplex virus type 1 (HSV-1) elicited a decrease in olfactory sensory neurons.

Conclusion: Our study provides new insights into a potential role for TRPM5-expressing cells in viral infection of the olfactory epithelium. We find that, as found for solitary chemosensory cells (SCCs) and brush cells in the airway epithelium, and for tuft cells in the intestine, the transcriptome of TRPM5-expressing microvillous cells and olfactory sensory neurons indicates that they are likely involved in the inflammatory response elicited by viral infection of the olfactory epithelium.

47 **Keywords:** Olfactory sensory neurons, Microvillous cells, Viral infection, Immunity,

48 Inflammation, Mouse

49 **Background**

50 Self-reported loss of smell in a large fraction of patients with coronavirus disease 2019 (COVID-
51 19), caused by severe acute respiratory syndrome coronavirus clade 2 (SARS-CoV-2),
52 (Giacomelli et al., 2020; Parma et al., 2020; Yan et al., 2020a; Yan et al., 2020b) raises the
53 question of how SARS-CoV-2 affects olfaction in a subset of patients. Entry of SARS-CoV-2
54 into cells is mediated by spike protein attachment to the SARS-CoV receptor ACE2 followed by
55 spike protein priming by the serine protease TMPRSS2 (Hoffmann et al., 2020). Chemosensory
56 cells found in the airway (SCCs/brush cells) and intestinal epithelium (tuft cells) express the
57 transient receptor potential cation channel subfamily M member 5 (TRPM5) and other elements
58 of the taste transduction pathway and have been implicated in immune and inflammatory
59 responses to bacterial, viral and parasitic infection (Luo et al., 2019; Maina et al., 2018; O'Leary
60 et al., 2019; Perniss et al., 2020; Rane et al., 2019; Saunders et al., 2014; Tizzano et al., 2010). In
61 the olfactory epithelium TRPM5 and other proteins involved in taste transduction are also
62 expressed in SCC-like microvillous cells (MVCs)(Genovese and Tizzano, 2018; Lin et al.,
63 2008), which have been proposed to be involved in a protective response to high concentrations
64 of odorants (Fu et al., 2018; Lemons et al., 2017). The ACE2 receptor and TMPRSS2 are
65 expressed in support cells, stem cells, and MVCs (Brann et al., 2020; Fodoulian et al., 2020).
66 However, whether MVCs play a role in viral infection or viral infection defense of the olfactory
67 epithelium is unknown.

68

69 Herein, we performed transcriptional profiling of MVCs and a subset of olfactory sensory
70 neurons (OSNs) expressing eGFP under control of the TRPM5 promoter (OSN_eGFP+
71 cells)(Lin et al., 2007; Lopez et al., 2014). In order to profile these low abundance cells we used

72 a modified version of Probe-Seq, which allows deep transcriptional profiling of specific cell
73 types identified by fluorescent markers as the defining feature (Amamoto et al., 2019). We
74 crossed a mouse expressing mCherry in the nuclei of OSNs under control of the OMP promoter
75 (OMP-H2B::mCherry mice) with TRPM5-eGFP transgenic mice (Clapp et al., 2006) (OMP-
76 H2B::mCherry/TRPM5-eGFP mice). We isolated cells from the olfactory epithelium and used
77 fluorescence-activated cell sorting (FACS) to sort MVC_eGFP cells (mCherry negative and
78 eGFP positive) and cells labeled by OMP-driven mCherry that did or did not express eGFP
79 (OSN_eGFP+ and OSN_eGFP- cells) followed by transcriptional profiling by RNA sequencing
80 (RNAseq).
81
82

83 **Results**

84

85 **Fluorescence-activated cell sorting of cells isolated from the main olfactory epithelium.** The
86 olfactory epithelium of OMP-H2B::mCherry/TRPM5-eGFP mice expressed nuclear mCherry
87 driven by the OMP promoter in the intermediate layer of the olfactory epithelium (Figures 1a), as
88 expected for the location of nuclei of mature OSNs (Farbman and Margolis, 1980). eGFP
89 expression driven by the TRPM5 promoter was found in MVCs, with cell bodies located mostly
90 in the apical layer of the epithelium (asterisks), and at lower expression levels in a subset of
91 OSNs double-labeled with mCherry (Figure 1a), consistent with earlier publications (Lin et al.,
92 2008; Lin et al., 2007; Pyrski et al., 2017).

93

94 We proceeded to isolate cells from the main olfactory epithelium of OMP-
95 H2B::mCherry/TRPM5-eGFP mice (see Methods, Figure 1b). Figure 1c shows two isolated
96 OSNs with differential expression of eGFP. Using flow cytometry we found that fluorescence
97 intensity of individual cells for mCherry and eGFP spanned several orders of magnitude (Figure
98 1d). We proceeded to sort three groups of cells: high mCherry-expressing cells with low and
99 high eGFP fluorescence (presumably mature OSNs, these cells are termed OSN_eGFP- and
100 OSN_eGFP+ cells respectively) and cells with low mCherry and high eGFP expression
101 (MVC_eGFP, presumably MVCs). Reverse transcription quantitative PCR (RT-qPCR) showed
102 that, as expected the OSN_eGFP- and OSN_eGFP+ cells have higher levels of OMP transcript
103 than MVC_eGFP cells (Figure 1e,i), and OSN_eGFP+ cells and MVC_eGFP cells have higher
104 levels of eGFP transcript compared to OSN_eGFP- cells (Figure 1e,ii). Furthermore, compared
105 to OSN_eGFP- cells both the MVC_eGFP cells and OSN_eGFP+ cells expressed higher levels

106 of TRPM5 transcript (Figure 1e,iii) and choline acetyl transferase (ChAT)(Figure 1e,iv), a
107 protein involved in acetylcholine neurotransmission that is expressed in MVCs (Ogura et al.,
108 2011). The asterisks in Figure 1e denote significant differences tested with either t-test or
109 ranksum with p-values below the p-value of significance corrected for multiple comparisons
110 using the false discovery rate (pFDR)(Curran-Everett, 2000) (pFDR is 0.033 for OMP, 0.05 for
111 TRPM5, 0.05 for EGFP and 0.03 for ChAT, n=8 for OMP OSN_eGFP-, 4 for OMP
112 OSN_eGFP+ and 4 for MVC_eGFP cells).
113
114 **The number of OSN_eGFP+ cells sorted by FACS is decreased when OMP-**
115 **H2B::mCherry/TRPM5-eGFP mice are placed in ventilated cages.** In our vivarium we have
116 ventilated cages (HV cages) where air is mechanically exchanged with fresh air once every
117 minute and static cages (LV cages) where air is exchanged passively through a filter in the cover.
118 When we moved the OMP-H2B::mCherry/TRPM5-eGFP to HV cages we noticed a decrease in
119 the number of OSN_eGFP+ cells sorted per mouse (Figures 2a,b and c), suggesting that changes
120 in ventilation conditions affect TRPM5 promoter-driven expression of eGFP. Following this
121 observation, mice were moved back to LV cages. We proceeded to study the dependence of the
122 number of OSN_eGFP+ cells sorted on the number of days in LV vs. HV cages. The number of
123 OSN_eGFP+ cells is positively correlated with the number of days the animal spends in LV
124 cages (Figure 2d) and negatively correlated to the number of days the animals spend in the HV
125 cages (Figure 2e). Generalized linear model (GLM) analysis found significant differences for the
126 number of OSN_eGFP+ cells sorted as a function of the number of days in LV cages ($p<0.05$, 26
127 observations, 24 d.f., F-statistic = 5.64, p-value for GLM <0.05) and the number of days in HV
128 cages ($p<0.05$, 26 observations, 24 d.f., F-statistic = 5.99, p-value for GLM <0.05). For RNAseq

129 experiments one FACS sort was done using cells from mice born and maintained in HV housing,
130 and the OSN_eGFP+ yield was low. Subsequently, we performed all FACS with cells isolated
131 from the olfactory epithelium of mice raised in LV cages.
132
133 **Coverage of TRPM5 transcript by RNAseq encompasses the full transcript in MVC_eGFP**
134 **cells and OSN_eGFP+ cells.** Pyrski and co-workers did not find full-length TRPM5 transcript
135 in reverse transcriptase polymerase chain reactions with mRNA extracted from isolated OSNs
136 from the adult mouse and did not find *in situ* signal in the OSN layer of the olfactory epithelium
137 for the full-length TRPM5 transcript (Pyrski et al., 2017). These investigators found full-length
138 TRPM5 transcript and strong *in situ* signal in MVCs. We find strong *in situ* signal for TRPM5 in
139 MVC_eGFP cells located in the apical layer of the olfactory epithelium (Figure 3aii, asterisks).
140 In addition, we find sparse TRPM5 *in situ* labeling in the nuclear OSN layer (Figure 3aii,
141 arrows). In order to gain a better understanding of which TRPM5 transcript is expressed in OSNs
142 we performed an analysis of TRPM5 transcript coverage for the RNAseq performed with RNA
143 from the different groups of cells sorted by FACS. Consistent with *in situ* labeling, TRPM5
144 transcript was significantly higher in OSN_eGFP+ cells compared to OSN_eGFP- cells and in
145 MVC_eGFP cells compared to OSN_eGFP- cells in both male and female adult mice (Figures
146 3b,c). To explore RNA sequencing coverage of individual *Trpm5* exons, we computed read
147 depth over the sequence of the *Trpm5* gene for each sample. We found coverage for all exons in
148 OSN_eGFP+ cells and for all exons except exon 1 and 5'UTR1 in MVC_eGFP cells, but there
149 was no coverage in OSN_eGFP- cells (Figures 3b,c). GLM analysis found statistically
150 significant differences for exons ($p<0.001$, 450 observations, 446 d.f., F-statistic = 33.8, p-value
151 for GLM <0.001), but no overall significance between MVC and OSN_eGFP+ groups ($p>0.05$,

152 450 observations, 446 d.f., F-statistic = 33.8, p-value for GLM <0.001). However, post-hoc
153 ranksum tests did yield significant differences between MVC and OSN_eGFP+ groups for exon
154 1 and 5'UTR1 (p<pFDR=0.0033). We observed no differences in coverage between male and
155 female mice (within MVC_eGFP cells: p>0.05, 210 observations, 206 d.f., F-statistic = 22.8, p
156 value for GLM <0.001; within OSN_GFP+: p>0.05, 240 observations, 236 d.f., F-statistic =
157 11.5, p value for GLM <0.001). Together, these data suggest that both OSN_eGFP+ cells and
158 MVC_eGFP cells are capable of expressing full-length TRPM5 transcript.
159
160 **RNAseq indicates that OSN_eGFP+, OSN_eGFP- and MVC are three distinct groups of**
161 **chemosensory cells in the mouse olfactory epithelium.** Differential gene expression analysis of
162 the RNAseq data was used to compare the three olfactory epithelium cell groups sorted by
163 FACS. We found that expression of 2000 genes was significantly higher in OSN_eGFP+
164 compared to OSN_eGFP-, and expression of 1821 genes was lower in OSN_eGFP+ cells (Figure
165 4 -figure supplement 1 shows the results of RNAseq and Figure 4 -figure supplement 2 shows
166 the metadata). Figure 4a shows expression levels for the transcripts that showed the largest
167 differences between OSN_eGFP+ and OSN_eGFP- cells. The transcripts for TRPM5 and eGFP
168 were among the top 10 genes whose transcription was higher in OSN_eGFP+ compared to
169 OSN_eGFP- with 105-fold and 42-fold increases respectively. This top 10 OSN_eGFP+
170 upregulated group also includes *Avil* and *Adgrg6* that are involved in remodeling processes after
171 peripheral nerve injury (Chuang et al., 2018; Jablonka-Shariff et al., 2020) and *Espn*, encoding
172 for espin, a protein playing a structural role in microvilli of chemosensory cells (Sekerkova et al.,
173 2004). Interestingly, the olfactory activity-dependent protein S100a5 (Fischl et al., 2014) is
174 found among the top 10 OSN_eGFP+ downregulated transcripts suggesting that in these mice

175 the OSN_eGFP+ are not stimulated by the odorants in their housing environment (Figure 4a).
176 Additionally, a majority of the olfactory receptors show decreased transcription in OSN_eGFP+
177 compared to OSN_eGFP- cells (Figures 4a,b) and the volcano plot for olfactory receptor
178 transcript expression shows only 25 olfactory receptors show increased expression in
179 OSN_eGFP+ cells (Figure 4c, based on fold change > 4 and average expression > 100 counts,
180 Table 1).
181
182 Expression of 4386 genes was significantly higher in MVC_eGFP cells compared to
183 OSN_eGFP- cells, and expression of 5630 genes was lower in MVC_eGFP cells (Figure 5 –
184 figure supplement 1). Transcripts for 550 olfactory receptors were lower in MVC_eGFP cells
185 (Figure 5 – figure supplement 1), and no olfactory receptors were upregulated in MVC_eGFP
186 cells compared to OSN_eGFP-. Figure 5a shows expression levels for the transcripts with the
187 largest differences between MVC_eGFP cells and OSN_eGFP- cells. Six of the transcripts that
188 are within the top 10 upregulated genes found in MVC_eGFP cells compared to OSN_eGFP-
189 cells (Figure 5a) are also found within the 10 top upregulated transcripts when OSN_eGFP+ cells
190 are compared to OSN_eGFP- cells (Figure 4a)(*Adgrg6*, *Avi*l, *Cd24a*, *eGFP*, *Espn* and *Trpm5*).
191 TRPM5 and eEGFP were among the top 10 genes whose transcription was higher in
192 MVC_eGFP cells compared to OSN_eGFP- cells with 1471-fold and 75-fold differences
193 respectively. Interestingly, *Pou2f3*, a transcription factor important in differentiation of MVCs
194 (Yamaguchi et al., 2014; Yamashita et al., 2017), is found within the top 10 upregulated genes
195 found in MVC_eGFP cells compared to OSN_eGFP- (Figure 5a) and is also significantly higher
196 in OSN_eGFP+ cells compared to OSN_eGFP- cells (Figure 5 – figure supplement 1). Finally,
197 *OMP* and *s100a5*, genes for two proteins expressed in mature OSNs (Farbman and Margolis,

198 1980; Fischl et al., 2014), were among the top 10 downregulated transcripts in MVC_eGFP cells
199 compared to OSN_eGFP- cells (Figure 5a).
200
201 We found expression of 3068 genes which was significantly higher in MVC_eGFP cells
202 compared to OSN_eGFP+ cells, and expression of 4060 genes was lower in MVC_eGFP cells
203 (Figure 5 – figure supplement 2). Figure 5b shows expression levels for the genes that showed
204 the largest differences between MVC and OSN_eGFP+ cells. Among the 10 genes that are
205 highly expressed in OSN_eGFP+ cells compared to MVC_eGFP cells we find *Pde4a,* a gene
206 expressed in mature OSNs (Juilfs et al., 1997) (*OMP* is also significantly higher in OSN_eGFP+
207 cells, but is not among the top 10 genes, Figure 5 – figure supplement 2). Interestingly, *Hcn2*, a
208 gene that encodes for a hyperpolarization-activated cAMP channel that has been postulated to
209 participate in OSN axon growth and glomerular innervation (Mobley et al., 2010), is found in the
210 top 10 upregulated OSN_eGFP+ genes. Finally, the gene encoding for the synaptic protein
211 Snap25 is found in the top 10 upregulated lists for both OSN_eGFP+ and OSN_eGFP- indicating
212 that both OSNs are involved in synaptic transmission (Figures 5a and b).
213
214 We did not find major differences in transcriptome profiling between males and females for
215 genes that were differentially expressed between the three cell groups (Figure 5 – figure
216 supplement 3,4). We found a substantial number of olfactory receptor genes that were
217 differentially expressed between males and females (Figure 5 – figure supplement 4).
218 Surprisingly, the differentially expressed olfactory receptors differed from receptors identified by
219 van der Linden et al. (van der Linden et al., 2018). Finally, we compared expression of
220 transcripts involved in taste transduction, canonical olfactory transduction, and non-canonical

221 OSNs (Figure 4d). The non-canonical OSNs considered here included guanilyl-cyclase D (GC-
222 D) OSNs (Juilfs et al., 1997), Trpc2 OSNs (Omura and Mombaerts, 2014) and Cav2.1 OSNs
223 (Pyrski et al., 2018). Both OSN_eGFP+ and OSN_eGFP- expressed low levels of *Cancna1a*
224 encoding for Cav2.1 and *Trpc2*. OSN_eGFP- expressed higher levels of Trace amine-associated
225 receptors (Liberles, 2015) than OSN_eGFP+ cells. Both OSN_eGFP+ and OSN_eGFP-
226 expressed transcripts for OMP, BBS1 and 2 and proteins involved in the canonical olfactory
227 transduction pathway, markers of canonical OSNs.
228
229 **Gene ontology enrichment analysis reveals differences in chemosensory transduction and**
230 **synaptic vesicle function between the three groups of cells.** Perusal of the top differences
231 between the three cell groups suggested that these are distinct chemosensory cell types found in
232 the olfactory epithelium. Both OSN_eGFP+ and OSN_eGFP- share expression of OSN-specific
233 transcripts, express distinct subsets of olfactory receptors and differ in expression of the activity-
234 dependent transcript *S100a5*, and MVC_eGFP cells differ from both OSN groups in expression
235 of transcripts for synaptic transmission and for markers of mature OSNs and microvillous cells.
236 In order to perform a thorough analysis of the differences between these chemosensory cell
237 groups we performed an analysis of gene ontology (GO) enrichment for lists of genes related to
238 chemosensory perception. When compared with either OSN_eGFP+ or OSN_eGFP- we found
239 that MVC_eGFP cells were enriched for transcripts for the gene ontology list of sensory
240 perception of sweet/umami taste (GO:0050916 and GO:0050917) (Figure 5d, Figure 5 – figure
241 supplements 3,4) involving taste detection/transduction proteins that have been reported to be
242 expressed in MVCs (Genovese and Tizzano, 2018; Hegg et al., 2010): *Gnat3*, encoding for
243 gustducin, the G protein mediating sweet and umami taste transduction (McLaughlin et al.,

244 1992), *Itpr3*, encoding for the inositol-1,4,5-triphosphate receptor type 3 and *Tas1r3*, encoding
245 for a gustducin-coupled receptor involved in umami and sweet taste (Damak et al., 2003; Zhang
246 et al., 2003). Interestingly, the GO lists for sensory perception of sweet/umami taste
247 (GO:0050916 and GO:0050917) and other lists for sensory and taste perception (GO:0050906,
248 GO:0050912) are enriched in OSN_eGFP+ cells compared to OSN_eGFP- cells (Figure 4e,
249 Figure 4 – figure supplement 3, including *Gnat3, Itpr3, Tas1r3*). Furthermore, gene ontology
250 analysis for OSN_eGFP+ cells compared to OSN_eGFP- cells finds decreased enrichment for
251 sensory perception of smell (GO:0007608) and G protein-coupled receptor signaling pathways
252 (GO:0007186) that include a large number of olfactory receptors and transcripts encoding for
253 proteins involved in peripheral olfaction such as *Gfy*, *Omp*, *Pde1c* and *Pde4a* (GO:0007608) and
254 *Dgkg*, *Gng13*, *Itgb1*, *Nsg1* (GO:0007186). Finally, enrichment of gene ontology lists for synaptic
255 vesicle function were decreased for MVC_eGFP cells compared with either OSN_eGFP+ or
256 OSN_eGFP- cells (Figure 5c,d). Results of this gene ontology analysis of chemosensation and
257 synaptic vesicle function reinforces the finding that the three cell groups in this study are distinct
258 chemosensory cell types of the olfactory epithelium. OSN_eGFP+ cells are related to
259 MVC_eGFP cells because of expression of taste perception gene ontology, but differ from
260 MVC_eGFP cells in expression of olfactory receptors and transcripts related to synaptic function
261 as expected for an OSN.
262
263 **Gene ontology analysis finds enrichment of lists of viral-related, inflammation and immune**
264 **transcripts in MVC_eGFP cells and OSN_eGFP+ cells.** SCCs, tuft and brush cells have been
265 implicated in responses to bacterial and viral infection, immunity and inflammation (Luo et al.,
266 2019; Maina et al., 2018; O'Leary et al., 2019; Perniss et al., 2020; Rane et al., 2019; Saunders et

267 al., 2014; Tizzano et al., 2010; Ualiyeva et al., 2020). The fact that MVCs are closely related to
268 these cells (Fu et al., 2018; Genovese and Tizzano, 2018; Ogura et al., 2011) lead us to search for
269 gene ontology enrichment related to bacterial and viral infection, immunity and inflammation for
270 MVC_eGFP cells. We found robust enrichment of these gene ontologies in MVC_eGFP cells
271 and OSN_eGFP+ cells (Figures 4e, 5c,d). Transcripts related to viral infection that were higher
272 in MVC_eGFP cells and OSN_eGFP+ cells compared to OSN_eGFP- cells (Figure 6) including
273 those involved in viral entry into host cells, viral transcription and regulation of viral
274 transcription, negative regulation of viral genome replication and negative regulation of viral
275 process (Figures 4e, 5c, Figure 6 – figure supplements 1-3). We also found gene ontology
276 enrichment in MVC_eGFP cells and OSN_eGFP+ cells compared to OSN_eGFP- cells for
277 defense response to bacterium (Figure 6 – figure supplements 1-3).
278
279 Importantly, we also find enrichment for transcript expression for immunity and inflammation
280 (Figures 4e, 5c,d and Figure 6 – figure supplements 1-3). Genes related to inflammation and
281 immunity that were higher in MVC_eGFP cells and OSN_eGFP+ cells compared to
282 OSN_eGFP- cells are shown in Figure 6 – figure supplements 4-7. Among these transcripts *IL25*
283 and its receptor *Il17rb* are enriched in both MVC_eGFP cells and OSN_eGFP+ cells. In SCCs,
284 brush cells and tuft cell generation of IL25 leads to a type 2 inflammation and stimulates
285 chemosensory cell expansion in a sequence of events that also involves cysteinyl leukotrienes
286 (Bankova et al., 2018; Luo et al., 2019; von Moltke et al., 2016). The presence of both *Il25* and
287 *Il17rb* suggests an autocrine effect. Furthermore, both cell types displayed increased expression
288 of transcripts encoding for enzymes involved in eicosanoid biosynthesis such as *Alox5*, *Ptgs1*

289 and *Ptgs2* that are found in brush cells in the airways (Bankova et al., 2018) and tuft cells in the
290 intestine (McGinty et al., 2020) where they drive type 2 immune responses.
291
292 **Acute infection with herpes simplex virus-1 (HSV-1) elicits a decrease in the fraction of**
293 **OSNs.** HSV-1 infects the olfactory epithelium in mice (Shivkumar et al., 2013). We found that
294 acute (5 DPI) high titer (1x 10^6 PFU/naris; McKrae strain) intranasal infection with HSV-1
295 elicited a decrease in the fraction of OSN_eGFP- and OSN_eGFP+ cells (Figure 7). GLM
296 analysis yielded significant effects for the fraction of OSN_eGFP- compared to MVCs ($p<0.001$)
297 and for the interaction between the fraction of OSN_eGFP- compared to MVCs and HSV-1 and
298 treatment ($p<0.001$, 75 observations, 69 d.f., GLM F-statistic=111 and p-value < 0.001, n=14
299 mice for control, n=11 mice for HSV-1 inoculation). Post-hoc t-test p-value was significant for
300 OSN_eGFP- and OSN_eGFP+ cells ($p < pFDR = 0.047$), but not for MVCs.
301
302
303
304
305

306 **Discussion**
307

308 We performed transcriptional profiling of three chemosensory cells in the mouse olfactory
309 epithelium: MVC_eGFP cells and two types of OSNs: OSN_eGFP+ and OSN_eGFP-. We found
310 that while the transcriptome of each of these cell types is distinct they share common features
311 across groups. The two groups of OSNs share transcript expression for proteins expressed in
312 OSNs such as OMP, olfactory transduction proteins, and proteins involved in synaptic function.
313 Yet, they differ in olfactory receptor expression and OSN_eGFP+ express taste transduction
314 transcripts and other transcripts found in SCCs such as *Il25* and *Pou2f3*. On the other hand,
315 MVC_eGFP cells express transcripts encoding for taste transduction proteins and other
316 transcripts found in SCCs such as *Pou2f3* but they do not express transcripts for proteins
317 involved in olfactory transduction and synaptic function, and they do not express olfactory
318 receptors. Finally, we found that MVC_eGFP cells and OSN_eGFP+ cells express a substantial
319 number of transcripts involved in viral infection, inflammation and immunity.
320

321 Here we find that OSN_eGFP+ are OSNs expressing full-length TRPM5 in the adult mouse
322 (Figure 3). This raises the question why our results differ from Pyrski and co-workers who did
323 not find full-length TRPM5 in OSNs (Pyrski et al., 2017). Likely, this is due to differences in
324 environmental conditions that alter the number of OSNs expressing TRPM5 in the adult mouse
325 (Figure 2). Interestingly, consistent with our finding of TRPM5 expression in OSNs, analysis of
326 scRNA data in the literature indicates that there are 8 OSNs expressing TRPM5 among 3209
327 OSNs in the data set from Ziegler and co-workers (Ziegler et al., 2020) and 3 OSNs expressing
328 TRPM5 among 2113 OSNs in the data set from Wu and co-workers (Wu et al., 2018). Finally,
329 OSN_eGFP+ express low levels of the activity-dependent transcript s100a5 (Fischl et al., 2014)

330 (Figure 4a) suggesting that these cells express olfactory receptors that are not stimulated by
331 odorants present in the cage.
332
333 Gene ontology analysis revealed that MVC_eGFP cells (and OSN_eGFP+ cells to a lesser
334 extent) are enriched in viral-related transcripts compared to OSN_eGFP- (Figures 4e, 5c,d, and
335 Figure 6 – figure supplements 1-3). To infect cells, viruses must interact with host cell
336 membranes to trigger membrane fusion and viral entry. Membrane proteins at the surface of the
337 host cell are thus key elements promoting or preventing viral infection. Here we find that
338 transcripts for several membrane proteins and cell adhesion molecules involved in viral entry are
339 enriched in MVC_eGFP cells. *Plscr1* encodes a phospholipid scramblase which has been shown
340 to promote herpes simplex virus (HSV) entry in human cervical or vaginal epithelial cells and
341 keratinocytes (Cheshenko et al., 2018), and hepatitis C virus entry into hepatocytes (Gong et al.,
342 2011). In contrast with its role in viral entry, PLSCR1 impairs the replication of other types of
343 viruses in infected cells (influenza A virus (Luo et al., 2018), hepatitis B virus (Yang et al.,
344 2012)). IFTM2 is another transmembrane protein that mediates viral entry. In contrast with
345 PLSCR1, IFTM2 inhibits viral entry of human immunodeficiency virus (HIV, (Yu et al., 2015)),
346 hepatitis C virus (Narayana et al., 2015), influenza A H1N1 virus, West Nile virus, and dengue
347 virus (Brass et al., 2009). IFTM2 also inhibits viral replication (Brass et al., 2009) and protein
348 synthesis (Lee et al., 2018). Nectins are transmembrane glycoproteins and constitute cell surface
349 receptors for numerous viruses. There is wide evidence that HSV can enter host cells through
350 Nectin-1 dependent mechanisms, particularly for neuronal entry (Kopp et al., 2009; Petermann et
351 al., 2015; Sayers and Elliott, 2016; Shukla et al., 2012), and Nectin-4 appears essential for
352 measles virus epithelial entry (Noyce and Richardson, 2012; Singh et al., 2015; Singh et al.,

353 2016). In addition to cell surface molecules, the mucus contains secreted proteins that confer
354 protection against viruses to the underlying cells. Glycoproteins are major constituents of mucus
355 and exhibit multiple pathogens binding-sites. We found the *Ltf* transcript in MVC_eGFP cells,
356 which encodes for lactotransferrin. Lactotransferrin is a globular glycoprotein widely represented
357 in the nasal mucus with anti-viral activity against Epstein-Barr virus (Zheng et al., 2014; Zheng
358 et al., 2012), HSV (Shestakov et al., 2012; Valimaa et al., 2009)) and Hepatitis C virus (Allaire et
359 al., 2015).
360
361 Viruses have developed numerous strategies to overcome barrier mechanisms to enter the cells.
362 After viral entry infected cells have other resources to fight against viral infection by disrupting
363 the production of new viral particles, limiting inflammation processes and activating innate
364 immune responses. For example, TRIM25 is an ubiquitin ligase that activates retinoic acid-
365 inducible gene I (RIG-I) to promote the antiviral interferon response (Gack et al., 2007).
366 Furthermore, influenza A virus targets TRIM25 to evade recognition by the host cell (Gack et al.,
367 2009). In addition, TRIM25 displays a nuclear role in restricting influenza A virus replication
368 (Meyerson et al., 2017). Zc3h12a, also known as MCPIP-1, inhibits hepatitis B and C virus
369 replication, reduces virus-induced inflammation (Li et al., 2020; Lin et al., 2014), and exerts
370 antiviral effects against influenza A virus (Dong et al., 2017). Finally, *Pou2f3* also called *Skn1a*,
371 encodes for a key regulator for the generation of TRPM5-expressing cells in various epithelial
372 tissues (Yamashita et al., 2017). *Pou2f3* transcript was increased in MVC_eGFP cells (and to a
373 lesser extent in OSN_eGFP+) compared to OSN_eGFP-. *Skn1a/Pou2f3*-deficient mice lack
374 intestinal tuft cells and have defective mucosal type 2 responses to helminth infection in the
375 intestine (Gerbe et al., 2016). Finally, both OSN_eGFP+ and MVC_eGFP cells express Il25, an

376 interleukin that is involved in the inflammatory response of TRPM5-expressing epithelial cells in
377 the airway epithelium and the gut (O'Leary et al., 2019), and in the skin Il25 expression leads to
378 disruption of the epithelium and enhances HSV-1 and vaccinia virus replication (Kim et al.,
379 2013).
380
381 Our findings of expression of virally relevant transcripts in MVC_eGFP cells complement
382 published studies on the role of MVC-related SCCs in viral infection. In the trachea, viral-
383 associated formyl peptides activate SCCs to release acetylcholine and activate mucocilliary
384 clearance by ciliated cells (Perniss et al., 2020). This activation is mediated by the TRPM5
385 transduction pathway in the SCC and muscarinic acetylcholine receptors in the ciliated cell. In a
386 similar manner in the olfactory epithelium MVCs respond to ATP, which is involved in
387 activating mucociliary movement by releasing acetylcholine and activating adjacent
388 sustentacular cells through a muscarinic receptor (Fu et al., 2018). Therefore, viral infection
389 could result in activation of MVCs resulting in activation of mucociliary clearance by adjacent
390 sustentacular cells. In addition, in the anterior olfactory epithelium, where there is a higher
391 density of MVCs, mice exposed to mild odorous irritants exhibited a time-dependent increase in
392 apoptosis and a loss of mature OSNs without a significant increase in proliferation or
393 neurogenesis (Lemons et al., 2020). This MVC-induced apoptosis could contribute to the
394 decrease in the fraction of OSNs elicited by intranasal inoculation of HSV-1 (Figure 7). Future
395 experiments are necessary to determine whether activation of MVCs by viruses could lead to loss
396 of mature OSNs contributing to smell loss after viral infection. We did not find changes in MVC
397 cell number after acute infection with HSV-1 (Figure 7c,iii). Interestingly, in the mouse distal
398 lung, where there is no expression of SCCs, there was de novo generation of SCCs after infection

399 with A/H1N1/PR/8 influenza virus (Rane et al., 2019) raising the question whether longer virus
400 exposure could alter MVC number in the olfactory epithelium. Finally, because we find high
401 expression of transcripts involved in Type 2 immune response in MVCs viral activation of these
402 cells could result in activation of cytokine-induced inflammation by long-term horizontal basal
403 cells that activate type 1 immune responses within the olfactory epithelium (Chen et al., 2019).
404
405 The olfactory epithelium provides direct viral access to the brain through the olfactory nerve.
406 Whether this olfactory path constitutes route of entry for viruses to the brain is a matter of
407 intense discussion, especially because some viruses are postulated to be involved in
408 encephalopathy and neurodegenerative disorders (Dando et al., 2014; Doty, 2008). Our findings
409 that these TRPM5-bearing OSN_eGFP+ cells are enriched in virally-related genes suggests that
410 these cells may be involved in or prevention of viral entry into the brain (and these two
411 alternatives are not exclusive since they may be different for different viruses). On the one hand,
412 we identified transcripts encoding for viral receptors in OSN_eGFP+ cells, suggesting that
413 viruses can enter these OSNs. If viral particles were to enter the OSNs they could reach the
414 olfactory bulb through anterograde transport along the olfactory nerve and from the olfactory
415 bulb, viruses can spread throughout the brain along the olfactory bulb-hippocampus route. On
416 the other hand, we found enrichment for transcripts encoding for proteins involved in limiting
417 viral infection and promoting immune and anti-inflammatory responses in OSNs_eGFP+ and
418 MVC_eGFP cells. In this case, viral spread to the brain would be prevented. Finally, the
419 olfactory epithelium is innervated by the trigeminal nerve, and substance P immunostaining is
420 closely associated with subsets of MVCs (Lin et al., 2008). This raises the question whether an
421 interaction between MVCs and trigeminal nerve fibers could participate in local inflammation as

422 found for SCCs (Saunders et al., 2014), and could modulate the entry of virus to the brain stem
423 through the trigeminal nerve. Future experiments are necessary to study the potential role of
424 MVC_eGFP cells and OSNs_eGFP+ in viral infection of the olfactory epithelium and the brain.
425
426 Recently, due to the current COVID-19 pandemic, researchers have focused their attention on
427 investigating SARS-CoV-2 mechanism of entry into cells. SARS-CoV-2 targets mainly cells of
428 the respiratory pathway where viral entry is mediated by ACE2 and TMPRSS2 (Hoffmann et al.,
429 2020). Because numerous patients reported loss of smell (Giacomelli et al., 2020; Parma et al.,
430 2020; Yan et al., 2020a; Yan et al., 2020b), researchers wondered about the mechanism for
431 SARS-CoV-2 infection of the olfactory epithelium. In our study, we found the *Tmprss2*
432 transcript was significantly increased in MVC_eGFP cells and OSN_eGFP+ compared to
433 OSN_eGFP- (Figure 6). We did not find *Ace2* enrichment in these cells, but this may be due to
434 inefficiency in finding with RNAseq low abundance transcripts like *Ace2* (Ziegler et al., 2020).
435 Transcriptional profiling of single cells in the olfactory epithelium from other laboratories found
436 expression of transcripts for both *Tmprss2* and *Ace2* in in sustentacular cells and stem cells, and
437 at lower levels in MVCs (Brann et al., 2020; Fodoulian et al., 2020). Viral infection of
438 sustentacular cells may explain loss of smell because these cells play a key role in supporting
439 olfactory function by providing glucose for the energy necessary for olfactory transduction in the
440 OSN cilia (Villar et al., 2017). Importantly, type I interferons, and to a lesser extent type II
441 interferons induced by response of the host to SARS-CoV-2, and infection by other viruses
442 inducing the interferon pathway increases *Ace2* expression in the nasal epithelium (Ziegler et al.,
443 2020). MVCs may play a role in SARS-CoV-2 infection of the olfactory epithelium because
444 these cells may participate in activating inflammation of the epithelium that elicits type 1

445 immune response (Chen et al., 2019). Finally, our finding of transcripts involved in viral entry,
446 replication and defense in a subset of OSNs raises the question whether viruses enter the central
447 nervous system through the olfactory nerve (Bilinska et al., 2020). This is relevant to the
448 potential long term effect of SARS-CoV-2 and other viruses in neurological and
449 neurodegenerative disorders (De Felice et al., 2020). Our study provides new insights into a
450 potential role for TRPM5-expressing cells in viral infection of the main olfactory epithelium.
451

452 **Conclusion**

453 Here we compared the transcriptome of OSNs that do not express TRPM5 (OSN_eGFP-) to a
454 small fraction of cells that express TRPM5 (MVC_eGFP cells and OSN_eGFP+ cells) in the
455 olfactory epithelium. We find that transcript expression in these three types of cells is distinct.
456 OSN_eGFP- and OSN_eGFP+ cells share transcripts expressed in OSNs, while OSN_eGFP+
457 and MVCs share expression of transcripts found in SCCs and brush cells in the airways and tuft
458 cells of the intestine. Interestingly, OSN_eGFP+ and MVCs express transcriptomes within the
459 gene ontology transcript groups for immunology, inflammation and viral infection.
460

461 **Abbreviations**

462 **COVID-19:** Coronavirus disease 2019

463 **DPI:** Days post infection

464 **eGFP:** Enhanced green fluorescent protein

465 **FACS:** Fluorescence-activated cell sorting

466 **FDR:** False discovery rate

467 **GLM:** Generalized linear model

468 **GO:** Gene ontology

469 **MVCs:** Microvillous cells

470 **OMP:** Olfactory marker protein

471 **OSNs:** Olfactory sensory neurons

472 **PSF:** Point spread function

473 **SARS-CoV-2:** Severe acute respiratory syndrome coronavirus clade 2

474 **SSC:** Saline-sodium citrate

475 **SSCT:** SSC with tween

476 **TRPM5:** Transient receptor potential cation channel subfamily M member 5

477 **Methods**

478 **Key Resources Table**

REAGENT TYPE	REAGENT or RESOURCE	SOURCE	IDENTIFIER	ADDITIONAL INFORMATION
Chemical compound, drug	BrainPhys Neuronal Medium	Stemcell Technologies		Product # 05791
Chemical compound, drug	Dispase II	Sigma		Product # D4693
Chemical compound, drug	AcGFP1/eGFP calibration beads	Takara		Flow cytometry calibration beads Product # 632594
Chemical compound, drug	mCherry calibration beads	Takara		Flow cytometry calibration beads Product # 632595
Chemical compound, drug	RQ1 RNase-free DNase	Promega		Product # M6101
Chemical compound, drug	Papain	Sigma		Product # P3125
Chemical compound, drug	Paraformaldehyde (32%)	Electron Microscopy Sciences		Product # 157145
Chemical compound, drug	RNAprotect Tissue Reagent	Qiagen		Product # 76526
Chemical compound, drug	RNeasy Plus Micro Kit	Qiagen		Product # 74034
Chemical compound, drug	High Capacity c-DNA Reverse Transcription kit	ABI		
Chemical compound, drug	18s rRNA	PE ABI		
Strain, strain background	TRPM5-eGFP	Dr. Robert Margolskee (Clapp et al., 2006)		
Strain, strain background	OMP-H2B::Cherry	Generated for this publication		This mouse will be deposited in Jackson Laboratories
Software, algorithm	MATLAB_R2018a	Mathworks	RRID: SCR_001622	
Software, algorithm	Illustrator	Adobe	RRID: SCR_010279	
Software, algorithm	Photoshop	Adobe	RRID: SCR_014199	

Software, algorithm	InDesign	Adobe		
Software, algorithm	MoFlo Astrios Summit Software (6.3.1.16945).	Beckman Coulter		
Software, algorithm	BBMap (BBDuk)		RRID:SCR_016968	
Software, algorithm	Salmon v1.2.1	https://combine-lab.github.io/salmon/	RRID:SCR_017036	(Patro et al., 2017)
Software, algorithm	DeSEQ2 v1.28.0	bioconductor.org https://bioconductor.org/packages/release/bioc/html/DESeq2.html	RRID:SCR_015687	(Love et al., 2014)
Software, algorithm	TopGO, v2.40.0		RRID:SCR_014798	
Software, algorithm	pHeatmap, 1.0.12		RRID:SCR_016418	
Software, algorithm	Ensembl GRCm38, v99			
Software, algorithm	R, v4.0		RRID:SCR_001905	
Software, algorithm	Tximport, v1.16.0		RRID:SCR_016752	
Software, algorithm	SAMtools	SAMtools http://samtools.sourceforge.net/	RRID:SCR_002105	(Li et al., 2009)
Software, algorithm	Bedtools		RRID:SCR_006646	
Software, algorithm	STAR v2.5.3a	https://github.com/alexdobin/STAR	RRID:SCR_015899	
Software, algorithm	Sigmaplot, v12.5	Systat Software	RRID:SCR_003210	
Software, algorithm	Custom code for bioinformatics analysis	https://github.com/eric-d-larson/OE_TRPM5		

479

480 **Overview of the method for transcriptional profiling of low abundance cell populations.** For
481 transcriptional profiling of TRPM5-bearing MVC_eGFP cells and OSN_eGFP+ cells that
482 constitute a small fraction of the cells in the epithelium, we used FACS to separate the cell
483 populations targeted for RNAseq (Amamoto et al., 2019). In our experiments, we isolated the
484 cells from mice that expressed fluorescent marker proteins appropriate for cell sorting. OSNs
485 were expressing mCherry under the control of OMP promoter. eGFP was expressed in MVCs
486 and a subset of OSNs (OSN_eGFP+ cells) under control of the TRPM5 promoter.
487
488 **Generation of OMP-H2B::Cherry mice**. A PacI cassette containing PacI-H2B::mCherry-pA
489 PGK-puro-pA-PacI was inserted into an OMP gene-targeting vector (pPM9)(Mombaerts et
490 al., 1996), which replaces the OMP coding sequence with the PacI cassette and expresses a
491 H2B::mCherry fusion protein. Animals are maintained in a mixed 129/B6 background.
492
493 **Animals.** Mice with TRPM5-driven eGFP expression (Clapp et al.,2006) were crossed with
494 OMP-H2B::Cherry mice. The TRPM5-eGFP mice were obtained with written informed consent
495 from Dr. Robert Margolskee. Both lines were maintained separately as homozygous and
496 backcrossed regularly. Experiments were performed on mice from the F1 generation cross of
497 TRPM5-eGFP and OMP-H2B::Cherry mice (OMP-H2B::mCherry/TRPM5-eGFP). PCR was
498 used to verify genotype of experimental mice for eGFP and mCherry expression. Both male and
499 female mice were used for experiments with ages ranging from 3- 8 months. Estrous and cage
500 mate information was collected for all female mice in conjunction with experimental use. Mice
501 were housed in passive air exchange caging under a 12:12 light/dark cycle and were given food
502 and water *ad libitum*. Mice were housed in the National Institutes of Health approved Center for

503 Comparative Medicine at the University of Colorado Anschutz Medical Campus. All procedures
504 were performed in compliance with University of Colorado Anschutz Medical Campus
505 Institutional Animal Care and Use Committee (IACUC) that reviews the ethics of animal use.
506
507 **Tissue dissociation of the olfactory epithelium.** Following euthanasia via CO2 inhalation, the
508 olfactory epithelium was immediately removed from the nasal cavity and epithelial tissue was
509 separated from the bone in the turbinates. Care was taken not to include respiratory epithelium.
510 The epithelium was dissociated enzymatically with Dispase II (2 mg/ml) diluted in Ringer's
511 solution (145mM NaCl, 5mM KCL, 20mM HEPES, 1mM $MgCL_2$, 1mM $CaCl_2$, 1mM Ny-
512 Pyruvate, 5mM Glucose) (~25 minutes at 37^0C) followed by an incubation in a papain plus
513 Ca/Mg++ free Ringer's solution (Ca/Mg++ free Ringer's: 145mM NaCl, 5mM KCL, 20mM
514 HEPES, 1mM Ny-Pyruvate, 1mM EDTA , L-cysteine: 1mg L-cysteine /1.5mL Ca/Mg++ free
515 Ringer's, Papain:1-3ul/1mL Ca/Mg++ free Ringer's), for ~40-45 minutes at 37^0C. Following
516 incubation, DNase I (Promega) at 0.05U/µl and RNAse free 10x Reaction buffer (1:20) were
517 added to solution and the tissue was gently triturated using a ~1mm opening pipette. Isolated
518 OSNs were collected from supernatants via centrifugation and resuspended in cell sorting
519 medium of 1x PBS (diluted from commercial 10x PBS, pH 7.4) and BrainPhys Neuronal
520 Medium (Stemcell Technologies). Initially, isolated cells were examined with a confocal
521 microscope to confirm efficacy of dissociation methods, and examine cell types and
522 fluorescence. For RNAseq, cells were strained through a 40 µm cell strainer and kept on ice until
523 sorted via flow cytometry.
524

525 **Flow cytometry.** Fluorescence activated cell sorting was performed in the University of
526 Colorado Cancer Center Flow Cytometry Core on a Beckman Coulter MoFlo Astrios EQ using
527 MoFlo Astrios Summit Software (6.3.1.16945). eGFP signal was detected using a 488 nm laser
528 and a bandpass 526/52nm collection filter. mCherry signal was detected using a 561 nm laser
529 and a bandpass 614/20 nm collection filter. The 488nm laser was also used to detect light
530 scatter. The threshold was set at 3%. Gating was set to exclude doublets and optimized as cell
531 populations emerged based on fluorescent markers. Flow cytometry calibration beads for
532 AcGFP1/eGFP and mCherry (Takara, 632594, 632595) were used as fluorescence intensity
533 controls. Olfactory epithelium cell suspensions from wild type and OMP-H2B::Cherry mice or
534 TRPM5-eGFP mice were sorted as controls for auto fluorescence for eGFP and mCherry
535 populations respectively. Cells were sorted into RNAprotect Tissue Reagent (Qiagen).
536
537 **RNA-extraction.** Total RNA was extracted from sorted, pooled cells from each cell population
538 using the RNeasy Plus Micro Kit (Qiagen) according to the manufacturers recommended
539 protocol.
540
541 **RT-qPCR.** Quantitative reverse transcription polymerase chain reaction (RT-qPCR) was used to
542 assess and confirm identities of cell types from each of the sorted cell populations. Following
543 total RNA extraction, RT-qPCR was performed in the PCR core at University of Colorado
544 Anschutz Medical Campus for the following markers: OMP, TRPM5, eGFP and ChAT. Primers
545 and probes used for eGFP, TRPM5 and OMP were described in (Oshimoto et al., 2013).
546 Predesigned primers and probes for ChAT were purchased from Life Technologies. The mRNA
547 for these targets was measured by RT-qPCR using ABI QuantStudio 7 flex Sequence detector.

548 1μg total RNA was used to synthesize cDNA using the High Capacity c-DNA Reverse
549 Transcription kit (ABI-P/N 4368814). cDNA was diluted 1: 2 before PCR amplification.
550
551 The TaqMan probes were 5'labeled with 6-carboxyfluorescein (FAM). Real time PCR reactions
552 were carried out in MicroAmp optical tubes (PE ABI) in a 25 μl mix containing 8 % glycerol,
553 1X TaqMan buffer A (500 mM KCl, 100 mM Tris-HCl, 0.1 M EDTA, 600 nM passive
554 reference dye ROX, pH 8.3 at room temperature), 300 μM each of dATP, dGTP, dCTP and 600
555 μM dUTP, 5.5 mM MgCl2, 1X primer-probe mix, 1.25 U AmpliTaq Gold DNA and 5 μl
556 template cDNA. Thermal cycling conditions were as follows: Initiation was performed at 50ºC
557 for 2 min followed by activation of TaqGold at 95ºC for 10 min. Subsequently 40 cycles of
558 amplification were performed at 95ºC for 15 secs and 60ºC for 1 min. Experiments were
559 performed with duplicates for each data point. Each PCR run included the standard curve (10
560 fold serially diluted pooled cDNA from control and experimental samples), test samples, no-
561 template and NORT controls. The standard curve was then used to calculate the relative
562 amounts of targets in test samples. Quantities of targets in test samples were normalized to the
563 corresponding 18s rRNA (PE ABI, P/N 4308310).
564
565 **RNA sequencing and pre-processing.** RNA quality control, library preparation, and sequencing
566 were performed at the University of Colorado Genomics and Microarray core. Extracted RNA
567 was used as the input for the Nugen Universal Plus mRNA-seq kit (Redwood City, CA) to build
568 stranded sequencing libraries. Indexed libraries were sequenced using an Illumina
569 NovaSEQ6000. Library preparation and sequencing was performed in two batches, separated by
570 gender. 11 female samples were sequenced with an average depth of 37.3 million +/- SD of 6.5

571 million read pairs, and 25 male samples were sequenced with an average depth of 34.8 million
572 +/- SD of 3.5 million read pairs. Metadata for the samples submitted are shown in Figure 4 –
573 figure supplement 2. Raw BCL files were demultiplexed and converted to FASTQ format.
574 Trimming, filtering, and adapter contamination removal was performed using BBDuk
575 (Bushnell).
576
577 **RNA Sequencing Analysis.** Transcript abundance was quantified from trimmed and filtered
578 FASTQ files using Salmon v1.2.1(Patro et al., 2017) and a customized Ensembl GRCm38
579 (release 99) transcriptome (Zerbino et al., 2018). A customized version of the transcriptome was
580 prepared by appending FASTA sequences of eGFP and mCherry to the GRCm38 FASTA file.
581 The corresponding gene transfer format (GTF) file was modified accordingly to incorporate the
582 new transcripts. Transcript abundance was summarized at the gene level using the TxImport
583 (Soneson et al., 2015) package in R. Differential gene expression was quantified using DESeq2
584 (Love et al., 2014) with default parameters after removing genes with an average count of < 5
585 reads in each group. Significance was determined by FDR-adjusted p-value < 0.05. TopGO was
586 used for gene ontology analysis (Alexa and Rahnenfuhrer, 2020). The input to TopGO was a list
587 of significant DEGs and a list of all detected genes in the dataset. Enrichment was calculated by
588 dividing the number of detected genes by the number of expected genes within each ontology of
589 the TopGO output. To make the bar graphs in Figures 4 and 5, enrichment scores of
590 downregulated GO terms were multiplied by -1 for visualization. Heatmap visualization was
591 performed using *pHeatmap* in R (Kolde, 2019).
592

593 **TRPM5 exon coverage.** To visualize exon coverage of *Trpm5*, trimmed and filtered FASTQ
594 files were mapped to the Ensembl GRCm38 (version 99) using STAR (params, version
595 2.5.3a)(Dobin et al., 2013). The genome FASTA and GTF files were modified as described
596 above. Read coverage was summarized by *Trpm5* exon using a combination of Samtools ('depth'
597 and 'bedcov')(Li et al., 2009) and Bedtools (Quinlan and Hall, 2010). Data were compared using
598 a Scheirer-Ray-Hare test in R (*rcompanion* package).
599
600 **Tissue Preparation for Fluorescence Microscopy and *in situ*.** For euthanasia, mice were
601 anesthetized with ketamine/xylazine (20–100 _g/g of body weight), perfused transcardially with
602 0.1 M phosphate buffer (PBS) followed by a PBS-buffered fixative (EMS 32%
603 Paraformaldehyde aqueous solution diluted to 4% with 1x PBS) . The nose was harvested and
604 postfixed for 12 h before being transferred for cryoprotection into PBS with 20% sucrose
605 overnight. The olfactory epithelium was cryosectioned coronally into 16 μm -thick sections
606 mounted on Superfrost Plus slides (VWR, West Chester, PA).
607
608 ***In situ.*** *In situ* hybridization was performed with the hybridization chain reaction method (Choi
609 et al., 2018) using HCR v3.0 Probe Sets, Amplifiers, and Buffers from Molecular Instruments,
610 Inc. Frozen slides were allowed to thaw and dry, then immersed in 70% ethanol overnight at
611 4°C, and allowed to dry again completely. Slides were inverted and placed on a Plexiglas
612 platform inside a humidified chamber; subsequent steps were performed using this setup. Slides
613 were incubated in 10 μg/μl proteinase K for 10 minutes at 37°C, then pre-hybridized with HCR
614 hybridization buffer (30% formamide buffer from Molecular Instruments) for 10 minutes at
615 37°C. *Trpm5-B3* probes and *OMP-B2* probes (0.4 pmol of each probe in 100 μl HCR

616 hybridization buffer per slide) were added, and slides were hybridized overnight at 37°C. Slides
617 were briefly incubated in undiluted HCR Wash Buffer (30% formamide buffer from Molecular
618 Instruments) at 37°C. Excess probes were removed by incubating slides for 15 minutes each at
619 37°C in solutions of 75% HCR Wash Buffer / 25% SSCT (5X SSC, 0.1% Tween, diluted in
620 RNAse free water), 50% Buffer / 50% SSCT, 25% Buffer / 75% SSCT, and 100% SSCT. Slides
621 were incubated in Amplification Buffer (Molecular Instruments) at room temperature for 30
622 minutes. B3 hairpins labeled with Alexa Fluor 647 and B2 hairpins labeled with Alexa Fluor 546
623 were prepared (6 pmol of each hairpin were heat shocked, then cooled for 30 minutes, and added
624 to 100µl of Amplification Buffer) added to slides, and incubated overnight at room temperature.
625 Excess hairpins were removed with three washes in SSCT at room temperature. Tissue was
626 counterstained with DAPI, and slides were mounted using Invitrogen SlowFade Diamond
627 Antifade Mountant (Thermo Fisher Scientific).
628
629 **Fluorescence microscopy.** Microscopy was performed with confocal microscopes (Nikon A1R
630 or 3i Marianas). Images shown are flattened Z stacks. In situ images in Figure 3 were
631 deconvolved in DeconvolutionLab 2 (Sage et al., 2017) using 10 rounds of Lucy-Richardson
632 deconvolution (Lucy, 1974; Richardson, 1972) and a theoretical point spread function (PSF).
633 The theoretical PSF was calculated using the Gibson-Lanni model (Gibson and Lanni, 1989) for
634 325 nm lateral and 800 nm axial pixel size, wavelength of the reporter dye molecule, and an air-
635 immersion 20X NA 0.75 objective. Image was maximum projected and Gamma of 0.8 applied to
636 the TRMP5 channel for viewing.
637

638 **Viral stocks.** HSV-1, McKrae strain (gift from Dr. David Bloom, University of Florida), was
639 used for all experiments. Viral stocks were prepared in Vero cells; infectious particles were
640 purified from the supernatant, aliquoted, and stored at -80C. Viral titers were determined via
641 plaque forming unit-(PFU) assays.
642
643 **Viral infection.** 3-6 month old OMP-H2B::mCherry/TRPM5-eGFP mice were lightly
644 anesthetized with isoflurane and inoculated intranasally with 10 μL of solution per naris (20 μL
645 total). The solution contained either HSV-1 (1x 10^6 PFU/naris; McKrae strain), or PBS (7.4 pH)
646 (sham control). Mice were randomly assigned to these groups. Mice were sacrificed at 5 days
647 post-infection (5 DPI). Controls included sham-treated mice (5), mice that were lightly
648 anesthetized (3), untreated mice housed in the BSL-2 facility (3) or the regular room (3). All
649 controls were used because ranksum tests corrected for multiple comparisons did not find
650 differences between these groups.
651
652 **Statistical analysis.** Statistical analysis was performed in Matlab (Mathworks, USA). Statistical
653 significance was estimated using a generalized linear model (GLM), with post-hoc tests for all
654 data pairs corrected for multiple comparisons using false discovery rate (Curran-Everett, 2000).
655 The post hoc comparisons between pairs of data were performed either with a t-test, or a ranksum
656 test, depending on the result of an Anderson-Darling test of normality. 95% CIs shown in the
657 figures as vertical black lines or shading bounding the lines were estimated by bootstrap analysis
658 of the mean by sampling with replacement 1000 times using the bootci function in MATLAB.
659
660
661

662 **Declarations**

663

664 ***Ethics approvals.*** Mouse experiments were carried out under guidelines of the National
665 Institutes of Health in compliance with University of Colorado Anschutz Medical Campus
666 Institutional Animal Care and Use Committee (IACUC).

667

668 ***Consent for publication.*** Not applicable.

669

670 ***Availability of data and materials.*** All data sequencing data are available in NCBI SRA
671 https://www.ncbi.nlm.nih.gov/sra/PRJNA632936. The code used for bioinformatics analysis is
672 found in https://github.com/eric-d-larson/OE_TRPM5

673

674 ***Competing interests.*** The authors declare no competing interests.

675

676 ***Funding.*** This work was supported by NIDCD DC014253 and NIA DC014253-04S1 (DR) and
677 by the RNA Bioscience Initiative of the University of Colorado Anschutz Medical Campus (DS
678 and DR). A Starr Stem Cell Grant (JA, AKH and PF) supported the production and
679 characterization of the OMP-H2B::mCherry mouse strain. The funding bodies had no role in the
680 experimental design or collection, analysis and interpretation of data or in writing the
681 manuscript.

682

683 **Authors' contributions.** D.R., B.D.B., M.N. and V.R. conceptualized the project. B.D.B.
684 performed FACS, qPCR and RNAseq experiments. E.D.L. performed genomic analysis. P.F.

generated the OMP-H2B::Cherry mice. D.S. designed and analyzed in situ experiments. M.N., A.N.B. and C.N. designed the HSV-1 inoculation experiments. C.N. and J.H.Jr. performed the viral inoculation. M.L. performed literature search and wrote the section on viral infection in the discussion. All authors contributed to writing and editing the manuscript.

Acknowledgements: We would like to acknowledge the support of Nicole Arevalo for laboratory support, Jerome Artus and Anna-Katerina Hadjantonakis for the construction of the targeting vector and production of OMP-H2B::Cherry mice.

Declaration of interests: The authors declare no competing interests.

696 **References**

697 Alexa, A., and Rahnenfuhrer, J. (2020). topGO: Enrichment Analysis for Gene Ontology (R
698 Package).

699 Allaire, A., Picard-Jean, F., and Bisaillon, M. (2015). Immunofluorescence to Monitor the
700 Cellular Uptake of Human Lactoferrin and its Associated Antiviral Activity Against the Hepatitis
701 C Virus. J Vis Exp.

702 Amamoto, R., Garcia, M.D., West, E.R., Choi, J., Lapan, S.W., Lane, E.A., Perrimon, N., and
703 Cepko, C.L. (2019). Probe-Seq enables transcriptional profiling of specific cell types from
704 heterogeneous tissue by RNA-based isolation. Elife *8*.

705 Bankova, L.G., Dwyer, D.F., Yoshimoto, E., Ualiyeva, S., McGinty, J.W., Raff, H., von Moltke,
706 J., Kanaoka, Y., Frank Austen, K., and Barrett, N.A. (2018). The cysteinyl leukotriene 3 receptor
707 regulates expansion of IL-25-producing airway brush cells leading to type 2 inflammation. Sci
708 Immunol *3*.

709 Bilinska, K., Jakubowska, P., Von Bartheld, C.S., and Butowt, R. (2020). Expression of the
710 SARS-CoV-2 Entry Proteins, ACE2 and TMPRSS2, in Cells of the Olfactory Epithelium:
711 Identification of Cell Types and Trends with Age. ACS Chemical Neuroscience.

712 Brann, D.H., Tsukahara, T., Weinreb, C., Lipovsek, M., Van den Berge, K., Gong, B., Chance,
713 R., Macaulay, I.C., Chou, H.-j., Fletcher, R.*, et al.* (2020). Non-neuronal expression of SARS-

714 CoV-2 entry genes in the olfactory system suggests mechanisms underlying COVID-19-
715 associated anosmia. bioRxiv, 2020.2003.2025.009084.

716 Brass, A.L., Huang, I.C., Benita, Y., John, S.P., Krishnan, M.N., Feeley, E.M., Ryan, B.J.,
717 Weyer, J.L., van der Weyden, L., Fikrig, E.*, et al.* (2009). The IFITM proteins mediate cellular
718 resistance to influenza A H1N1 virus, West Nile virus, and dengue virus. Cell *139*, 1243-1254.

719 Bushnell, B. BBMap (SourceForge).

720 Chen, M., Reed, R.R., and Lane, A.P. (2019). Chronic Inflammation Directs an Olfactory Stem
721 Cell Functional Switch from Neuroregeneration to Immune Defense. Cell Stem Cell *25*, 501-513
722 e505.

723 Cheshenko, N., Pierce, C., and Herold, B.C. (2018). Herpes simplex viruses activate
724 phospholipid scramblase to redistribute phosphatidylserines and Akt to the outer leaflet of the
725 plasma membrane and promote viral entry. PLoS Pathog *14*, e1006766.

726 Choi, H.M., Schwarzkopf, M., Fornace, M.E., Acharya, A., Artavanis, G., Stegmaier, J., Cunha,
727 A., and Pierce, N.A. (2018). Third-generation in situ hybridization chain reaction: multiplexed,
728 quantitative, sensitive, versatile, robust. Development *145*, dev165753.

729 Chuang, Y.C., Lee, C.H., Sun, W.H., and Chen, C.C. (2018). Involvement of advillin in
730 somatosensory neuron subtype-specific axon regeneration and neuropathic pain. Proc Natl Acad
731 Sci U S A *115*, E8557-E8566.

732 Clapp, T.R., Medler, K.F., Damak, S., Margolskee, R.F., and Kinnamon, S.C. (2006). Mouse
733 taste cells with G protein-coupled taste receptors lack voltage-gated calcium channels and
734 SNAP-25. BMC Biol *4*, 7.

735 Curran-Everett, D. (2000). Multiple comparisons: philosophies and illustrations. AmJPhysiol
736 RegulIntegrComp Physiol *279*, R1-R8.

737 Damak, S., Rong, M., Yasumatsu, K., Kokrashvili, Z., Varadarajan, V., Zou, S., Jiang, P.,
738 Ninomiya, Y., and Margolskee, R.F. (2003). Detection of sweet and umami taste in the absence
739 of taste receptor T1r3. Science *301*, 850-853.

740 Dando, S.J., Mackay-Sim, A., Norton, R., Currie, B.J., St John, J.A., Ekberg, J.A.K., Batzloff,
741 M., Ulett, G.C., and Beacham, I.R. (2014). Pathogens Penetrating the Central Nervous System:
742 Infection Pathways and the Cellular and Molecular Mechanisms of Invasion. Clinical
743 Microbiology Reviews *27*, 691-726.

744 De Felice, F.G., Tovar-Moll, F., Moll, J., Munoz, D.P., and Ferreira, S.T. (2020). Severe Acute
745 Respiratory Syndrome Coronavirus 2 (SARS-CoV-2) and the Central Nervous System. Trends in
746 Neurosciences.

747 Dobin, A., Davis, C.A., Schlesinger, F., Drenkow, J., Zaleski, C., Jha, S., Batut, P., Chaisson,
748 M., and Gingeras, T.R. (2013). STAR: ultrafast universal RNA-seq aligner. Bioinformatics *29*,
749 15-21.

750 Dong, C., Sun, X., Guan, Z., Zhang, M., and Duan, M. (2017). Modulation of influenza A virus
751 replication by microRNA-9 through targeting MCPIP1. J Med Virol *89*, 41-48.

752 Doty, R.L. (2008). The olfactory vector hypothesis of neurodegenerative disease: is it viable?
753 Ann Neurol *63*, 7-15.

754 Farbman, A.I., and Margolis, F.L. (1980). Olfactory marker protein during ontogeny:
755 immunohistochemical localization. Developmental biology *74*, 205-215.

756 Fischl, A.M., Heron, P.M., Stromberg, A.J., and McClintock, T.S. (2014). Activity-dependent
757 genes in mouse olfactory sensory neurons. Chem Senses *39*, 439-449.

758 Fodoulian, L., Tuberosa, J., Rossier, D., Landis, B.N., Carleton, A., and Rodriguez, I. (2020).
759 SARS-CoV-2 receptor and entry genes are expressed by sustentacular cells in the human
760 olfactory neuroepithelium. bioRxiv, 2020.2003.2031.013268.

761 Fu, Z., Ogura, T., Luo, W., and Lin, W. (2018). ATP and Odor Mixture Activate TRPM5-
762 Expressing Microvillous Cells and Potentially Induce Acetylcholine Release to Enhance
763 Supporting Cell Endocytosis in Mouse Main Olfactory Epithelium. Front Cell Neurosci *12*, 71.

764 Gack, M.U., Albrecht, R.A., Urano, T., Inn, K.S., Huang, I.C., Carnero, E., Farzan, M., Inoue,
765 S., Jung, J.U., and Garcia-Sastre, A. (2009). Influenza A virus NS1 targets the ubiquitin ligase
766 TRIM25 to evade recognition by the host viral RNA sensor RIG-I. Cell Host Microbe *5*, 439-
767 449.

768 Gack, M.U., Shin, Y.C., Joo, C.H., Urano, T., Liang, C., Sun, L., Takeuchi, O., Akira, S., Chen,
769 Z., Inoue, S.*, et al.* (2007). TRIM25 RING-finger E3 ubiquitin ligase is essential for RIG-I-
770 mediated antiviral activity. Nature *446*, 916-920.

771 Genovese, F., and Tizzano, M. (2018). Microvillous cells in the olfactory epithelium express
772 elements of the solitary chemosensory cell transduction signaling cascade. PLoS One *13*,
773 e0202754.

774 Gerbe, F., Sidot, E., Smyth, D.J., Ohmoto, M., Matsumoto, I., Dardalhon, V., Cesses, P.,
775 Garnier, L., Pouzolles, M., Brulin, B.*, et al.* (2016). Intestinal epithelial tuft cells initiate type 2
776 mucosal immunity to helminth parasites. Nature *529*, 226-230.

777 Giacomelli, A., Pezzati, L., Conti, F., Bernacchia, D., Siano, M., Oreni, L., Rusconi, S.,
778 Gervasoni, C., Ridolfo, A.L., Rizzardini, G.*, et al.* (2020). Self-reported olfactory and taste
779 disorders in SARS-CoV-2 patients: a cross-sectional study. Clin Infect Dis.

780 Gibson, S.F., and Lanni, F. (1989). Diffraction by a circular aperture as a model for three-
781 dimensional optical microscopy. J Opt Soc Am A *6*, 1357-1367.

782 Gong, Q., Cheng, M., Chen, H., Liu, X., Si, Y., Yang, Y., Yuan, Y., Jin, C., Yang, W., He, F.*, et*
783 *al.* (2011). Phospholipid scramblase 1 mediates hepatitis C virus entry into host cells. FEBS Lett
784 *585*, 2647-2652.

785 Hegg, C.C., Jia, C., Chick, W.S., Restrepo, D., and Hansen, A. (2010). Microvillous cells
786 expressing IP3 receptor type 3 in the olfactory epithelium of mice. Eur J Neurosci *32*, 1632-
787 1645.

788 Hoffmann, M., Kleine-Weber, H., Schroeder, S., Kruger, N., Herrler, T., Erichsen, S.,
789 Schiergens, T.S., Herrler, G., Wu, N.H., Nitsche, A.*, et al.* (2020). SARS-CoV-2 Cell Entry
790 Depends on ACE2 and TMPRSS2 and Is Blocked by a Clinically Proven Protease Inhibitor. Cell
791 *181*, 271-280 e278.

792 Jablonka-Shariff, A., Lu, C.Y., Campbell, K., Monk, K.R., and Snyder-Warwick, A.K. (2020).
793 Gpr126/Adgrg6 contributes to the terminal Schwann cell response at the neuromuscular junction
794 following peripheral nerve injury. Glia *68*, 1182-1200.

795 Juilfs, D.M., Fulle, H.J., Zhao, A.Z., Houslay, M.D., Garbers, D.L., and Beavo, J.A. (1997). A
796 subset of olfactory neurons that selectively express cGMP-stimulated phosphodiesterase (PDE2)
797 and guanylyl cyclase-D define a unique olfactory signal transduction pathway. Proc Natl Acad
798 Sci U S A *94*, 3388-3395.

799 Kim, B.E., Bin, L., Ye, Y.M., Ramamoorthy, P., and Leung, D.Y.M. (2013). IL-25 enhances
800 HSV-1 replication by inhibiting filaggrin expression, and acts synergistically with Th2 cytokines
801 to enhance HSV-1 replication. J Invest Dermatol *133*, 2678-2685.

802 Kolde, R. (2019). pheatmap: Pretty Heatmaps (cran.r-project.org).

803 Kopp, S.J., Banisadr, G., Glajch, K., Maurer, U.E., Grunewald, K., Miller, R.J., Osten, P., and
804 Spear, P.G. (2009). Infection of neurons and encephalitis after intracranial inoculation of herpes
805 simplex virus requires the entry receptor nectin-1. Proc Natl Acad Sci U S A *106*, 17916-17920.

806 Lee, W.J., Fu, R.M., Liang, C., and Sloan, R.D. (2018). IFITM proteins inhibit HIV-1 protein
807 synthesis. Sci Rep *8*, 14551.

808 Lemons, K., Fu, Z., Aoude, I., Ogura, T., Sun, J., Chang, J., Mbonu, K., Matsumoto, I.,
809 Arakawa, H., and Lin, W. (2017). Lack of TRPM5-Expressing Microvillous Cells in Mouse
810 Main Olfactory Epithelium Leads to Impaired Odor-Evoked Responses and Olfactory-Guided
811 Behavior in a Challenging Chemical Environment. eNeuro *4*.

812 Lemons, K., Fu, Z., Ogura, T., and Lin, W. (2020). TRPM5-expressing Microvillous Cells
813 Regulate Region-specific Cell Proliferation and Apoptosis During Chemical Exposure.
814 Neuroscience *434*, 171-190.

815 Li, H., Handsaker, B., Wysoker, A., Fennell, T., Ruan, J., Homer, N., Marth, G., Abecasis, G.,
816 Durbin, R., and Genome Project Data Processing, S. (2009). The Sequence Alignment/Map
817 format and SAMtools. Bioinformatics *25*, 2078-2079.

818 Li, M., Yang, J., Zhao, Y., Song, Y., Yin, S., Guo, J., Zhang, H., Wang, K., Wei, L., Li, S*., et al.*
819 (2020). MCPIP1 inhibits Hepatitis B virus replication by destabilizing viral RNA and negatively
820 regulates the virus-induced innate inflammatory responses. Antiviral Res *174*, 104705.

821 Liberles, S.D. (2015). Trace amine-associated receptors: ligands, neural circuits, and behaviors.
822 Current opinion in neurobiology *34*, 1-7.

823 Lin, R.J., Chu, J.S., Chien, H.L., Tseng, C.H., Ko, P.C., Mei, Y.Y., Tang, W.C., Kao, Y.T.,
824 Cheng, H.Y., Liang, Y.C.*, et al.* (2014). MCPIP1 suppresses hepatitis C virus replication and
825 negatively regulates virus-induced proinflammatory cytokine responses. J Immunol *193*, 4159-
826 4168.

827 Lin, W., Ezekwe, E.A., Jr., Zhao, Z., Liman, E.R., and Restrepo, D. (2008). TRPM5-expressing
828 microvillous cells in the main olfactory epithelium. BMC Neurosci *9*, 114.

829 Lin, W., Margolskee, R., Donnert, G., Hell, S.W., and Restrepo, D. (2007). Olfactory neurons
830 expressing transient receptor potential channel M5 (TRPM5) are involved in sensing
831 semiochemicals. Proc Natl Acad Sci U S A *104*, 2471-2476.

832 Lopez, F., Delgado, R., Lopez, R., Bacigalupo, J., and Restrepo, D. (2014). Transduction for
833 Pheromones in the Main Olfactory Epithelium Is Mediated by the Ca2+-Activated Channel
834 TRPM5. J Neurosci *34*, 3268-3278.

835 Love, M.I., Huber, W., and Anders, S. (2014). Moderated estimation of fold change and
836 dispersion for RNA-seq data with DESeq2. Genome Biol *15*, 550.

837 Lucy, L.B. (1974). An iterative technique for the rectification of observed distributions. The
838 Astronomical Journal *79*, 745.

839 Luo, W., Zhang, J., Liang, L., Wang, G., Li, Q., Zhu, P., Zhou, Y., Li, J., Zhao, Y., Sun, N., *et al.*
840 (2018). Phospholipid scramblase 1 interacts with influenza A virus NP, impairing its nuclear
841 import and thereby suppressing virus replication. PLoS Pathog *14*, e1006851.

842 Luo, X.C., Chen, Z.H., Xue, J.B., Zhao, D.X., Lu, C., Li, Y.H., Li, S.M., Du, Y.W., Liu, Q.,
843 Wang, P., *et al.* (2019). Infection by the parasitic helminth Trichinella spiralis activates a Tas2r-
844 mediated signaling pathway in intestinal tuft cells. Proc Natl Acad Sci U S A *116*, 5564-5569.

845 Maina, I.W., Workman, A.D., and Cohen, N.A. (2018). The role of bitter and sweet taste
846 receptors in upper airway innate immunity: Recent advances and future directions. World J
847 Otorhinolaryngol Head Neck Surg *4*, 200-208.

848 McGinty, J.W., Ting, H.-A., Billipp, T.E., Nadjsombati, M.S., Khan, D.M., Barrett, N.A., Liang,
849 H.-E., Matsumoto, I., and von Moltke, J. (2020). Tuft-Cell-Derived Leukotrienes Drive Rapid
850 Anti-helminth Immunity in the Small Intestine but Are Dispensable for Anti-protist Immunity.
851 Immunity *52*, 528-541.e527.

852 McLaughlin, S.K., McKinnon, P.J., and Margolskee, R.F. (1992). Gustducin is a taste-cell-
853 specific G protein closely related to the transducins. Nature *357*, 563-569.

854 Meyerson, N.R., Zhou, L., Guo, Y.R., Zhao, C., Tao, Y.J., Krug, R.M., and Sawyer, S.L. (2017).
855 Nuclear TRIM25 Specifically Targets Influenza Virus Ribonucleoproteins to Block the Onset of
856 RNA Chain Elongation. Cell Host Microbe *22*, 627-638 e627.

857 Mobley, A.S., Miller, A.M., Araneda, R.C., Maurer, L.R., Muller, F., and Greer, C.A. (2010).
858 Hyperpolarization-activated cyclic nucleotide-gated channels in olfactory sensory neurons
859 regulate axon extension and glomerular formation. The Journal of neuroscience : the official
860 journal of the Society for Neuroscience *30*, 16498-16508.

861 Mombaerts, P., Wang, F., Dulac, C., Chao, S.K., Nemes, A., Mendelsohn, M., Edmondson, J.,
862 and Axel, R. (1996). Visualizing an olfactory sensory map. Cell *87*, 675-686.

863 Narayana, S.K., Helbig, K.J., McCartney, E.M., Eyre, N.S., Bull, R.A., Eltahla, A., Lloyd, A.R.,
864 and Beard, M.R. (2015). The Interferon-induced Transmembrane Proteins, IFITM1, IFITM2,
865 and IFITM3 Inhibit Hepatitis C Virus Entry. J Biol Chem *290*, 25946-25959.

866 Noyce, R.S., and Richardson, C.D. (2012). Nectin 4 is the epithelial cell receptor for measles
867 virus. Trends Microbiol *20*, 429-439.

868 O'Leary, C.E., Schneider, C., and Locksley, R.M. (2019). Tuft Cells-Systemically Dispersed
869 Sensory Epithelia Integrating Immune and Neural Circuitry. Annu Rev Immunol *37*, 47-72.

870 Ogura, T., Szebenyi, S.A., Krosnowski, K., Sathyanesan, A., Jackson, J., and Lin, W. (2011).
871 Cholinergic microvillous cells in the mouse main olfactory epithelium and effect of acetylcholine
872 on olfactory sensory neurons and supporting cells. J Neurophysiol *106*, 1274-1287.

873 Omura, M., and Mombaerts, P. (2014). Trpc2-Expressing Sensory Neurons in the Main
874 Olfactory Epithelium of the Mouse. Cell Reports *8*, 583-595.

875 Oshimoto, A., Wakabayashi, Y., Garske, A., Lopez, R., Rolen, S., Flowers, M., Arevalo, N., and
876 Restrepo, D. (2013). Potential role of transient receptor potential channel M5 in sensing putative
877 pheromones in mouse olfactory sensory neurons. PLoS One *8*, e61990.

878 Parma, V., Ohla, K., Veldhuizen, M.G., Nim, M.Y., Kelly, C.E., Reed, D.R., Hummel, T.,
879 Munger, S., and Hayes, J.E. (2020). More than just smell - COVID-19 is associated with severe
880 impairment of smell, taste, and chemesthesis. medRxiv, 2020.2005.2004.20090902.

881 Patro, R., Duggal, G., Love, M.I., Irizarry, R.A., and Kingsford, C. (2017). Salmon provides fast
882 and bias-aware quantification of transcript expression. Nature methods *14*, 417-419.

883 Perniss, A., Liu, S., Boonen, B., Keshavarz, M., Ruppert, A.L., Timm, T., Pfeil, U., Soultanova,
884 A., Kusumakshi, S., Delventhal, L.*, et al.* (2020). Chemosensory Cell-Derived Acetylcholine
885 Drives Tracheal Mucociliary Clearance in Response to Virulence-Associated Formyl Peptides.
886 Immunity *52*, 683-699 e611.

887 Petermann, P., Rahn, E., Thier, K., Hsu, M.J., Rixon, F.J., Kopp, S.J., and Knebel-Morsdorf, D.
888 (2015). Role of Nectin-1 and Herpesvirus Entry Mediator as Cellular Receptors for Herpes
889 Simplex Virus 1 on Primary Murine Dermal Fibroblasts. J Virol *89*, 9407-9416.

890 Pyrski, M., Eckstein, E., Schmid, A., Bufe, B., Weiss, J., Chubanov, V., Boehm, U., and Zufall,
891 F. (2017). Trpm5 expression in the olfactory epithelium. Mol Cell Neurosci *80*, 75-88.

892 Pyrski, M., Tusty, M., Eckstein, E., Oboti, L., Rodriguez-Gil, D.J., Greer, C.A., and Zufall, F.
893 (2018). P/Q Type Calcium Channel Cav2.1 Defines a Unique Subset of Glomeruli in the Mouse
894 Olfactory Bulb. Frontiers in Cellular Neuroscience *12*, 295.

895 Quinlan, A.R., and Hall, I.M. (2010). BEDTools: a flexible suite of utilities for comparing
896 genomic features. Bioinformatics *26*, 841-842.

897 Rane, C.K., Jackson, S.R., Pastore, C.F., Zhao, G., Weiner, A.I., Patel, N.N., Herbert, D.R.,
898 Cohen, N.A., and Vaughan, A.E. (2019). Development of solitary chemosensory cells in the
899 distal lung after severe influenza injury. Am J Physiol Lung Cell Mol Physiol *316*, L1141-
900 L1149.

901 Richardson, W.H. (1972). Bayesian-Based Iterative Method of Image Restoration*. J Opt Soc
902 Am *62*, 55-59.

903 Sage, D., Donati, L., Soulez, F., Fortun, D., Schmit, G., Seitz, A., Guiet, R., Vonesch, C., and
904 Unser, M. (2017). DeconvolutionLab2: An open-source software for deconvolution microscopy.
905 Methods *115*, 28-41.

906 Saunders, C.J., Christensen, M., Finger, T.E., and Tizzano, M. (2014). Cholinergic
907 neurotransmission links solitary chemosensory cells to nasal inflammation. Proc Natl Acad Sci U
908 S A *111*, 6075-6080.

909 Sayers, C.L., and Elliott, G. (2016). Herpes Simplex Virus 1 Enters Human Keratinocytes by a
910 Nectin-1-Dependent, Rapid Plasma Membrane Fusion Pathway That Functions at Low
911 Temperature. J Virol *90*, 10379-10389.

912 Sekerkova, G., Zheng, L., Loomis, P.A., Changyaleket, B., Whitlon, D.S., Mugnaini, E., and
913 Bartles, J.R. (2004). Espins are multifunctional actin cytoskeletal regulatory proteins in the
914 microvilli of chemosensory and mechanosensory cells. J Neurosci *24*, 5445-5456.

915 Shestakov, A., Jenssen, H., Nordstrom, I., and Eriksson, K. (2012). Lactoferricin but not
916 lactoferrin inhibit herpes simplex virus type 2 infection in mice. Antiviral Res *93*, 340-345.

917 Shivkumar, M., Milho, R., May, J.S., Nicoll, M.P., Efstathiou, S., and Stevenson, P.G. (2013).
918 Herpes simplex virus 1 targets the murine olfactory neuroepithelium for host entry. J Virol *87*,
919 10477-10488.

920 Shukla, N.D., Tiwari, V., and Valyi-Nagy, T. (2012). Nectin-1-specific entry of herpes simplex
921 virus 1 is sufficient for infection of the cornea and viral spread to the trigeminal ganglia. Mol Vis
922 *18*, 2711-2716.

923 Singh, B.K., Hornick, A.L., Krishnamurthy, S., Locke, A.C., Mendoza, C.A., Mateo, M., Miller-
924 Hunt, C.L., Cattaneo, R., and Sinn, P.L. (2015). The Nectin-4/Afadin Protein Complex and
925 Intercellular Membrane Pores Contribute to Rapid Spread of Measles Virus in Primary Human
926 Airway Epithelia. J Virol *89*, 7089-7096.

927 Singh, B.K., Li, N., Mark, A.C., Mateo, M., Cattaneo, R., and Sinn, P.L. (2016). Cell-to-Cell
928 Contact and Nectin-4 Govern Spread of Measles Virus from Primary Human Myeloid Cells to
929 Primary Human Airway Epithelial Cells. J Virol *90*, 6808-6817.

930 Soneson, C., Love, M.I., and Robinson, M.D. (2015). Differential analyses for RNA-seq:
931 transcript-level estimates improve gene-level inferences. F1000Res *4*, 1521.

932 Tizzano, M., Gulbransen, B.D., Vandenbeuch, A., Clapp, T.R., Herman, J.P., Sibhatu, H.M.,
933 Churchill, M.E., Silver, W.L., Kinnamon, S.C., and Finger, T.E. (2010). Nasal chemosensory
934 cells use bitter taste signaling to detect irritants and bacterial signals. Proc Natl Acad Sci U S A
935 *107*, 3210-3215.

936 Ualiyeva, S., Hallen, N., Kanaoka, Y., Ledderose, C., Matsumoto, I., Junger, W.G., Barrett,
937 N.A., and Bankova, L.G. (2020). Airway brush cells generate cysteinyl leukotrienes through the
938 ATP sensor P2Y2. Science Immunology *5*, eaax7224.

939 Valimaa, H., Tenovuo, J., Waris, M., and Hukkanen, V. (2009). Human lactoferrin but not
940 lysozyme neutralizes HSV-1 and inhibits HSV-1 replication and cell-to-cell spread. Virol J *6*, 53.

941 van der Linden, C., Jakob, S., Gupta, P., Dulac, C., and Santoro, S.W. (2018). Sex separation
942 induces differences in the olfactory sensory receptor repertoires of male and female mice. Nat
943 Commun *9*, 5081.

944 Villar, P.S., Delgado, R., Vergara, C., Reyes, J.G., and Bacigalupo, J. (2017). Energy
945 Requirements of Odor Transduction in the Chemosensory Cilia of Olfactory Sensory Neurons
946 Rely on Oxidative Phosphorylation and Glycolytic Processing of Extracellular Glucose. J
947 Neurosci *37*, 5736-5743.

948 von Moltke, J., Ji, M., Liang, H.E., and Locksley, R.M. (2016). Tuft-cell-derived IL-25 regulates
949 an intestinal ILC2-epithelial response circuit. Nature *529*, 221-225.

950 Wu, Y., Ma, L., Duyck, K., Long, C.C., Moran, A., Scheerer, H., Blanck, J., Peak, A., Box, A.,
951 Perera, A.*, et al.* (2018). A Population of Navigator Neurons Is Essential for Olfactory Map
952 Formation during the Critical Period. Neuron *100*, 1066-1082 e1066.

953 Yamaguchi, T., Yamashita, J., Ohmoto, M., Aoude, I., Ogura, T., Luo, W., Bachmanov, A.A.,
954 Lin, W., Matsumoto, I., and Hirota, J. (2014). Skn-1a/Pou2f3 is required for the generation of
955 Trpm5-expressing microvillous cells in the mouse main olfactory epithelium. BMC Neurosci *15*,
956 13.

957 Yamashita, J., Ohmoto, M., Yamaguchi, T., Matsumoto, I., and Hirota, J. (2017). Skn-1a/Pou2f3
958 functions as a master regulator to generate Trpm5-expressing chemosensory cells in mice. PLoS
959 One *12*, e0189340.

960 Yan, C.H., Faraji, F., Prajapati, D.P., Boone, C.E., and DeConde, A.S. (2020a). Association of
961 chemosensory dysfunction and Covid-19 in patients presenting with influenza-like symptoms.
962 Int Forum Allergy Rhinol.

963 Yan, C.H., Faraji, F., Prajapati, D.P., Ostrander, B.T., and DeConde, A.S. (2020b). Self-reported
964 olfactory loss associates with outpatient clinical course in Covid-19. Int Forum Allergy Rhinol.

965 Yang, J., Zhu, X., Liu, J., Ding, X., Han, M., Hu, W., Wang, X., Zhou, Z., and Wang, S. (2012).
966 Inhibition of Hepatitis B virus replication by phospholipid scramblase 1 in vitro and in vivo.
967 Antiviral Res *94*, 9-17.

968 Yu, J., Li, M., Wilkins, J., Ding, S., Swartz, T.H., Esposito, A.M., Zheng, Y.M., Freed, E.O.,
969 Liang, C., Chen, B.K.*, et al.* (2015). IFITM Proteins Restrict HIV-1 Infection by Antagonizing
970 the Envelope Glycoprotein. Cell Rep *13*, 145-156.

971 Zerbino, D.R., Achuthan, P., Akanni, W., Amode, M.R., Barrell, D., Bhai, J., Billis, K.,
972 Cummins, C., Gall, A., Giron, C.G.*, et al.* (2018). Ensembl 2018. Nucleic Acids Res *46*, D754-
973 D761.

974 Zhang, Y., Hoon, M.A., Chandrashekar, J., Mueller, K.L., Cook, B., Wu, D., Zuker, C.S., and
975 Ryba, N.J. (2003). Coding of sweet, bitter, and umami tastes: different receptor cells sharing
976 similar signaling pathways. Cell *112*, 293-301.

977 Zheng, Y., Qin, Z., Ye, Q., Chen, P., Wang, Z., Yan, Q., Luo, Z., Liu, X., Zhou, Y., Xiong, W.*,*
978 *et al.* (2014). Lactoferrin suppresses the Epstein-Barr virus-induced inflammatory response by
979 interfering with pattern recognition of TLR2 and TLR9. Lab Invest *94*, 1188-1199.

980 Zheng, Y., Zhang, W., Ye, Q., Zhou, Y., Xiong, W., He, W., Deng, M., Zhou, M., Guo, X.,
981 Chen, P., *et al.* (2012). Inhibition of Epstein-Barr virus infection by lactoferrin. J Innate Immun
982 *4*, 387-398.

983 Ziegler, C.G.K., Allon, S.J., Nyquist, S.K., Mbano, I.M., Miao, V.N., Tzouanas, C.N., Cao, Y.,
984 Yousif, A.S., Bals, J., Hauser, B.M., *et al.* (2020). SARS-CoV-2 receptor ACE2 is an interferon-
985 stimulated gene in human airway epithelial cells and is detected in specific cell subsets across
986 tissues. Cell.
987

988 **Figure legends**

989

990 **Figure 1. Fluorescence activated sorting (FACS) of cells isolated from the olfactory**
991 **epithelium.**

992 **a.** TRPM5 promoter driven expression of eGFP and OMP promoter driven expression of
993 mCherry in the olfactory epithelium. Expression of eGFP is found both in MVCs that do not
994 express mCherry (asterisk) and in OSNs double labeled with eGFP and mCherry (arrow). **i.**
995 Composite, **ii.** eGFP, **iii.** mCherry, **iv**. Composite magnification. Magenta: mCherry, green:
996 eGFP. Scale bar: i-iii, 50 mm, iv, 10 mm.

997 **b.** Schematic of RNA-seq process from tissue to RNA extraction. Mouse OE was dissociated
998 into single cells and sorted via FACS. RNA was extracted from each of the resulting cell
999 populations.

1000 **c.** Two isolated OSNs differing in eGFP expression. Magenta: mCherry, green: eGFP. Scale bar:
1001 10 mm.

1002 **d.** Distribution of mCherry and eGFP fluorescence intensity for FACS-sorted cells. Three cell
1003 populations were isolated for RNAseq: Cells with low OMP promoter-driven mCherry
1004 expression and high TRPM5 promoter-driven eGFP expression (MVC_eGFP cells), cells with
1005 high OMP promoter-driven mCherry and low eGFP expression (OSN_eGFP- cells) and cells
1006 with eGFP expression of the same magnitude as MVC_eGFP cells and high OMP promoter-
1007 driven mCherry expression (OSN_eGFP+ cells). The number of cells collected for this FACS
1008 run were: OSN_eGFP-s 1,500,000, OSN_eGFP+s 5336 and MVC_eGFP cells 37,178.

1009 **e.** qPCR levels (normalized to levels 18s RNA) for expression of transcripts encoding for OMP
1010 (**i**), TRPM5 (**ii**), eGFP (**iii**) and ChAT (**iv**). The asterisks denote significant differences tested

1011 with either t-test or ranksum with p-values below the significance p-value corrected for multiple
1012 comparisons using the false discovery rate (pFDR)(Curran-Everett, 2000). pFDR is 0.033 for
1013 OMP, 0.05 for TRPM5, 0.05 for eGFP and 0.03 for ChAT, n=8 for OMP OSN_eGFP-s, 4 for
1014 OMP OSN_eGFP+s and 4 for MVC_eGFP cells.
1015
1016 **Figure 2. Decreased yield of OSN_eGFP+ cells when mice are moved from low ventilation**
1017 **(LV) to high ventilation (HV) cages.**
1018 **a and b.** Distribution of mCherry and eGFP fluorescence intensity for FACS-sorted cells that
1019 either were not transferred to HV cages (**a**) or were transferred to HV cages for 22 days before
1020 sorting (**b**).
1021 **c.** Time course showing change in the number of sorted OSN_eGFP+s after mice were
1022 transferred to HV cages.
1023 **d and e.** Dependence of the yield of OSN_eGFP+ cells after sorting on the number of days in
1024 LV cages (**d**) or the number of days in HV cages (**e**).
1025
1026 **Figure 3. Coverage of TRPM5 transcript by RNAseq in the different cell groups sorted**
1027 **from the olfactory epithelium**
1028 **a.** In situ for TRPM5 and OMP transcripts in the olfactory epithelium shows strong label for
1029 TRPM5 in MVCs (asterisks) and sparse labeling in the OSN nuclear layer (arrows). **i.** OMP, **ii.**
1030 TRPM5, **iii.** Composite. The scale bar is 100 μm.
1031 **b and c.** Coverage of the reads for the TRPM5 transcript for the different cell groups. Read
1032 coverage was computed with 'Samtools depth' over the region corresponding to the Trpm5 gene.

1033 **b.** Coverage per exon. All samples normalized to TRPM5 reads show distribution among exons
1034 with little difference between MVC and OSN_eGFP+ cells.
1035 **c.** Coverage shown per base pair as a function of location in the genomic DNA. Plots show read
1036 depth per base pair for each cell type normalized to total number of mapped reads. Gray shading
1037 indicates 95% confidence interval.
1038
1039 **Figure 4. RNAseq comparison of OSN_eGFP- and OSN_eGFP+ cells.**
1040 **a.** Heatmap showing the top 10 upregulated and top 10 downregulated genes identified by
1041 DESeq2.
1042 **b.** Heatmap showing all *Olfr* genes detected in the data.
1043 For both a and b, row and column order were determined automatically by the *pHeatmap*
1044 package in R. For each data point relative expression was calculated by subtracting the average
1045 row value from each individual value.
1046 **c.** Volcano plot of all Olfactory receptors, demonstrating the small number of enriched olfactory
1047 receptors in the OSN_eGFP+ population.
1048 **d.** Hierarchical clustering of transcripts for taste transduction and transcripts expressed in
1049 canonical and non-canonical OSNs identified by RNAseq as significantly different in expression
1050 between the cell groups. We compared expression of transcripts involved in taste transduction,
1051 canonical olfactory transduction, and non-canonical OSNs. The non-canonical OSNs considered
1052 here included guanilyl-cyclase D (GC-D) OSNs (Juilfs et al., 1997), Trpc2 OSNs (Omura and
1053 Mombaerts, 2014), Cav2.1 OSNs (Pyrski et al., 2018), and OSNs expressing trace amine-
1054 associated receptors (Taars) (Liberles, 2015). Transcripts identified by DESeq2.

1055 **e.** Gene ontology (GO) term enrichment was calculated from differentially expressed genes using
1056 *TopGO* in R. An enrichment value for genes with Fischer p value <0.05 was calculated by
1057 dividing the number of expressed genes within the GO term by the number expected genes (by
1058 random sampling, determined by *TopGO*).
1059
1060 **Figure 5. RNAseq comparison of OSN_eGFP- and OSN_eGFP+ vs. MVC_eGFP cells.**
1061 **a and b.** Heatmaps showing hierarchical clustering of the top 10 upregulated and top 10
1062 downregulated genes identified by DESeq2. **a.** OSN_eGFP- vs. MVC_eGFP cells. **b**.
1063 OSN_eGFP+ vs. MVC_eGFP cells. For both a and b, row and column order were determined
1064 automatically by the *pHeatmap* package in R. For each data point relative expression was
1065 calculated by subtracting the average row value from each individual value.
1066 **c and d.** Gene ontology (GO) term enrichment was calculated from differentially expressed
1067 genes using *TopGO* in R. **c.** OSN_eGFP- vs. MVC_eGFP cells. **d**. OSN_eGFP+ vs.
1068 MVC_eGFP cells. An enrichment value for genes with Fischer p value <0.05 was calculated by
1069 dividing the number of expressed genes within the GO term by the number expected genes (by
1070 random sampling, determined by *TopGO*).
1071
1072 **Figure 6. Significant differences in virally-related gene ontology.** Heatmaps show hierarchical
1073 clustering of significantly differentially expressed genes identified by DESeq2. **a.** MVC_eGFP
1074 cells compared to OSN_eGFP-. **b.** OSN_eGFP+ compared to OSN_eGFP-.
1075

1076 **Figure 7. Intranasal inoculation with HSV-1 elicits a decrease in OSNs.**

1077 **a and b.** Distribution of mCherry and eGFP fluorescence intensity for FAC-sorted cells that

1078 either were not infected (**a**) or were inoculated intranasally with 10 μL of solution per naris (20

1079 μL total with HSV-1 (1x 10^6 PFU/naris; McKrae strain) 5 DPI (**b**).

1080 **c.** Fraction of total cells for OSN_eGFP- (**i**), OSN_eGFP+ (**ii**) or MVC (**iii**) cell groups. GLM

1081 analysis yielded significant effects for the fraction of OSN_eGFP- compared to MVCs ($p<0.001$)

1082 and for the interaction between the fraction of OSN_eGFP- compared to MVCs and HSV-1

1083 treatment ($p<0.001$, 75 observations, 69 d.f., GLM F-statistic=111 and p-value < 0.001, n=14

1084 mice for control, n=11 mice for HSV-1 inoculation). Asterisks denote a significant difference

1085 post-hoc with t-test p-value < pFDR = 0.047.

1086

1087

Name	OSN_eGFP-	OSN_eGFP+	MVC_eGFP	p-value adjusted
Olfr292	3.61	959	4.29	6.35E-09
Olfr282	2.05	486	0	8.01E-05
Olfr1434	53.3	7730	0	9.71E-16
Olfr390	101	10800	43.1	1.56E-16
Olfr305	6.14	612	0	6.3E-12
Olfr293	6.96	664	16.9	1.42E-07
Olfr378	3.41	322	0	1.1E-06
Olfr128	39.6	3660	12.7	7.33E-14
Olfr344	16.2	1050	0	1.4E-11
Olfr307	7.59	393	0	3.76E-06
Olfr391	156	8000	9.79	1.01E-15
Olfr299	13.1	651	0	4.58E-09
Olfr142	36.4	1720	3.77	1.62E-08
Olfr1	147	5720	52.7	3.08E-10
Olfr1279	16.4	552	10.9	3.52E-07
Olfr39	13.8	388	21	2.81E-06
Olfr1447	64.1	1610	0	1.23E-07
Olfr728	2150	45700	320	6.13E-22
Olfr727	560	11000	179	1.64E-07
Olfr1555-ps1	10.1	175	0	0.0397
Olfr346	27.6	465	0	3.85E-05
Olfr1228	533	5320	35.4	3.09E-08
Olfr1181	87.4	766	4.61	0.000766
Olfr943	97.1	844	2.89	0.000886
Olfr298	60.1	509	0	0.00132

Table 1. Levels of expression and adjusted p-value for the olfactory receptor genes whose levels are significantly higher in OSN_eGFP+ compared to OSN_eGFP-. These olfactory receptors had an adjusted p-value for expression level difference between OSN_eGFP+ compared to OSN_eGFP- and had a fold change > 4 and average expression > 100 counts.

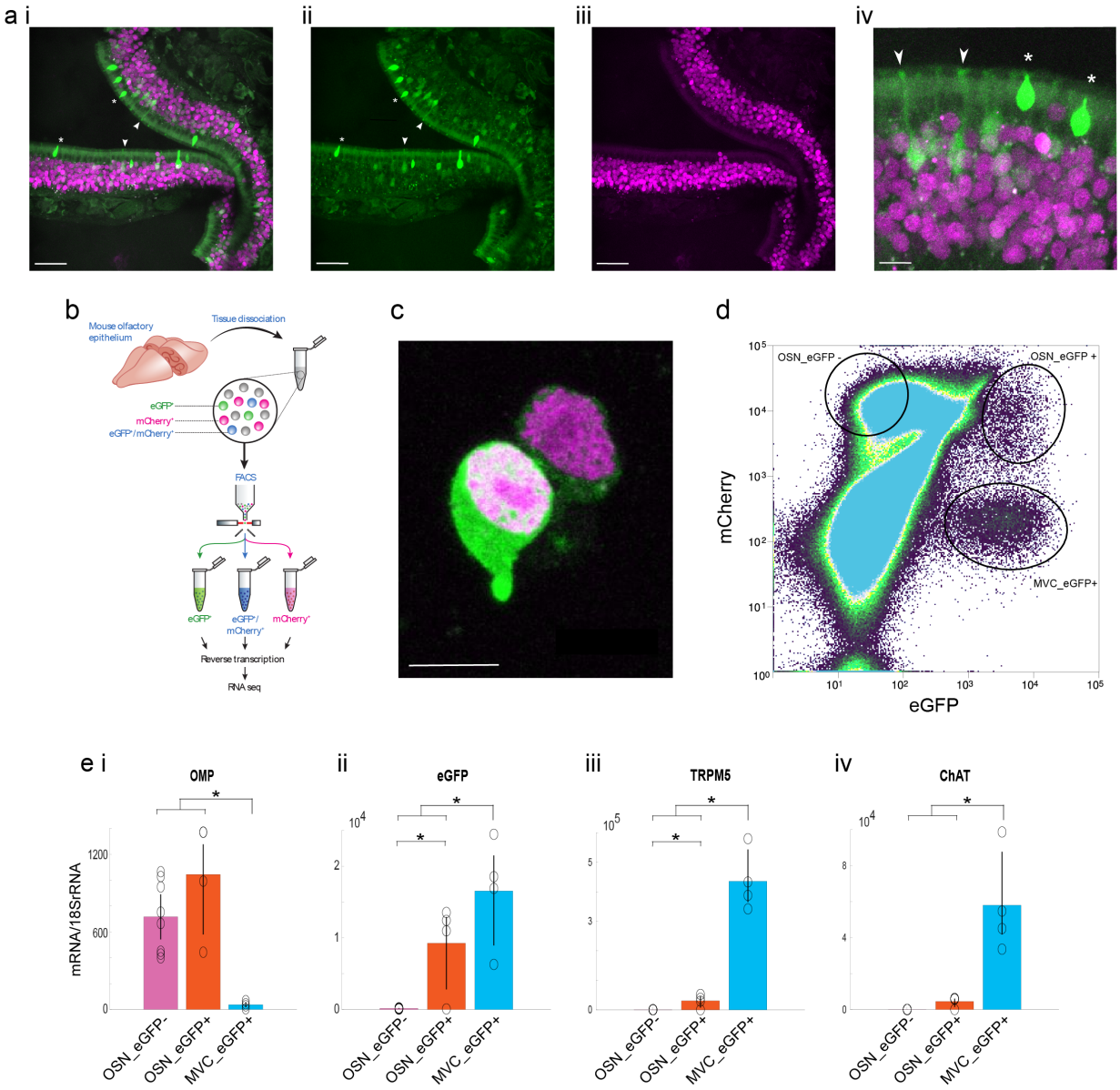

Figure 1. Fluorescence activated sorting (FACS) of cells isolated from the olfactory epithelium.

a. TRPM5 promoter driven expression of eGFP and OMP promoter driven expression of mCherry in the olfactory epithelium. Expression of eGFP is found both in MVCs that do not express mCherry (asterisk) and in OSNs double labeled with eGFP and mCherry (arrow). **i.** Composite, **ii.** eGFP, **iii.** mCherry, **iv**. Composite magnification. Magenta: mCherry, green: eGFP. Scale bar: i-iii, 50 µm, iv, 10 µm.

1104 **b.** Schematic of RNA-seq process from tissue to RNA extraction. Mouse OE was dissociated
1105 into single cells and sorted via FACS. RNA was extracted from each of the resulting cell
1106 populations.
1107 **c.** Two isolated OSNs differing in eGFP expression. Magenta: mCherry, green: eGFP. Scale bar:
1108 10 μm.
1109 **d.** Distribution of mCherry and eGFP fluorescence intensity for FACS-sorted cells. Three cell
1110 populations were isolated for RNAseq: Cells with low OMP promoter-driven mCherry
1111 expression and high TRPM5 promoter-driven eGFP expression (MVC_eGFP cells), cells with
1112 high OMP promoter-driven mCherry and low eGFP expression (OSN_eGFP- cells) and cells
1113 with eGFP expression of the same magnitude as MVC_eGFP cells and high OMP promoter-
1114 driven mCherry expression (OSN_eGFP+ cells). The number of cells collected for this FACS
1115 run were: OSN_eGFP-s 1,500,000, OSN_eGFP+s 5336 and MVC_eGFP cells 37,178.
1116 **e.** qPCR levels (normalized to levels 18s RNA) for expression of transcripts encoding for OMP
1117 (**i**), TRPM5 (**ii**), eGFP (**iii**) and ChAT (**iv**). The asterisks denote significant differences tested
1118 with either t-test or ranksum with p-values below the significance p-value corrected for multiple
1119 comparisons using the false discovery rate (pFDR)(Curran-Everett, 2000). pFDR is 0.033 for
1120 OMP, 0.05 for TRPM5, 0.05 for eGFP and 0.03 for ChAT, n=8 for OMP OSN_eGFP-s, 4 for
1121 OMP OSN_eGFP+s and 4 for MVC_eGFP cells.
1122
1123

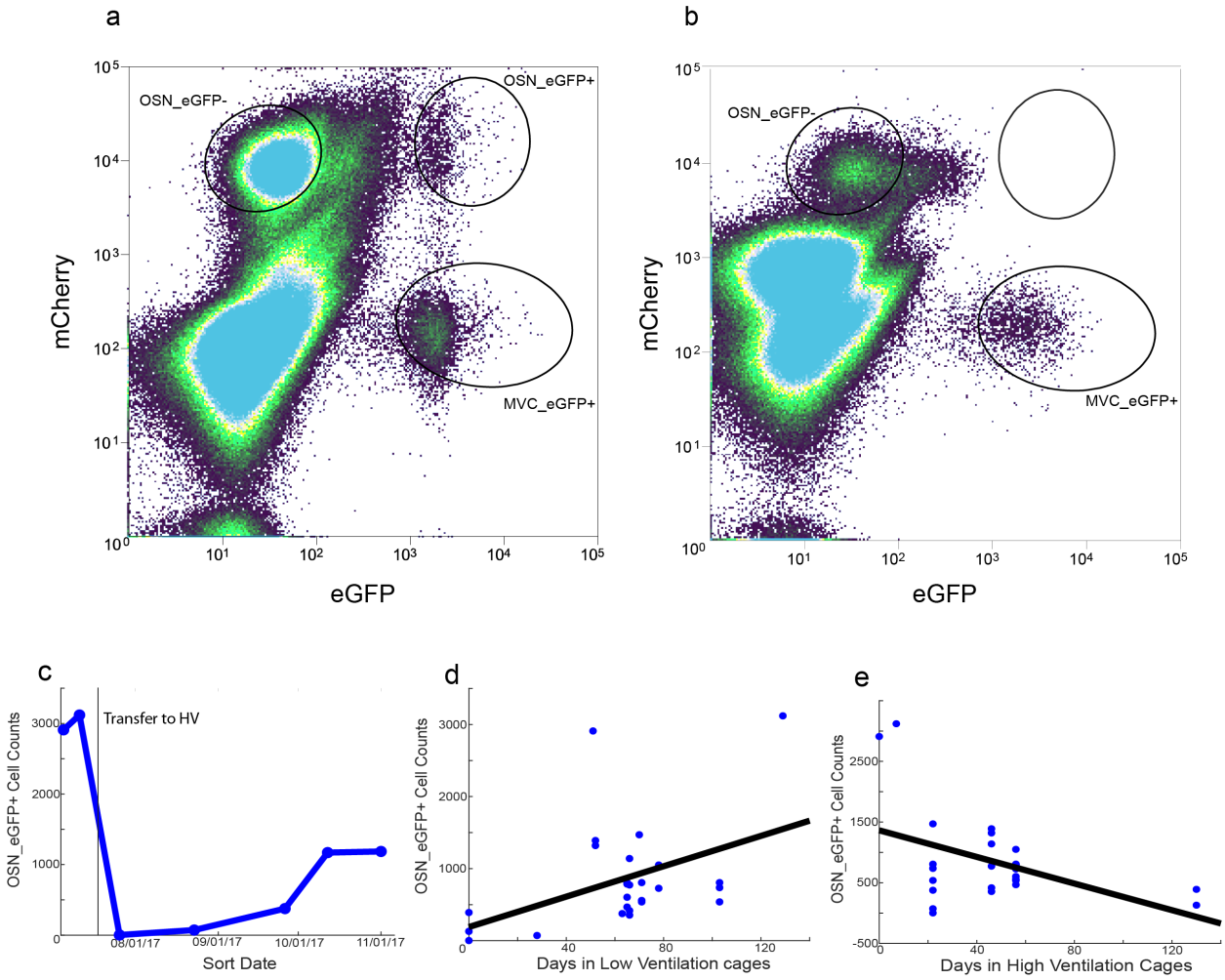

Figure 2. Decreased yield of OSN_eGFP+ cells when mice are moved from low ventilation (LV) to high ventilation (HV) cages.

a and b. Distribution of mCherry and eGFP fluorescence intensity for FACS-sorted cells that either were not transferred to HV cages (**a**) or were transferred to HV cages for 22 days before sorting (**b**).

c. Time course showing change in the number of sorted OSN_eGFP+s after mice were transferred to HV cages.

d and e. Dependence of the yield of OSN_eGFP+ cells after sorting on the number of days in LV cages (**d**) or the number of days in HV cages (**e**).

1134

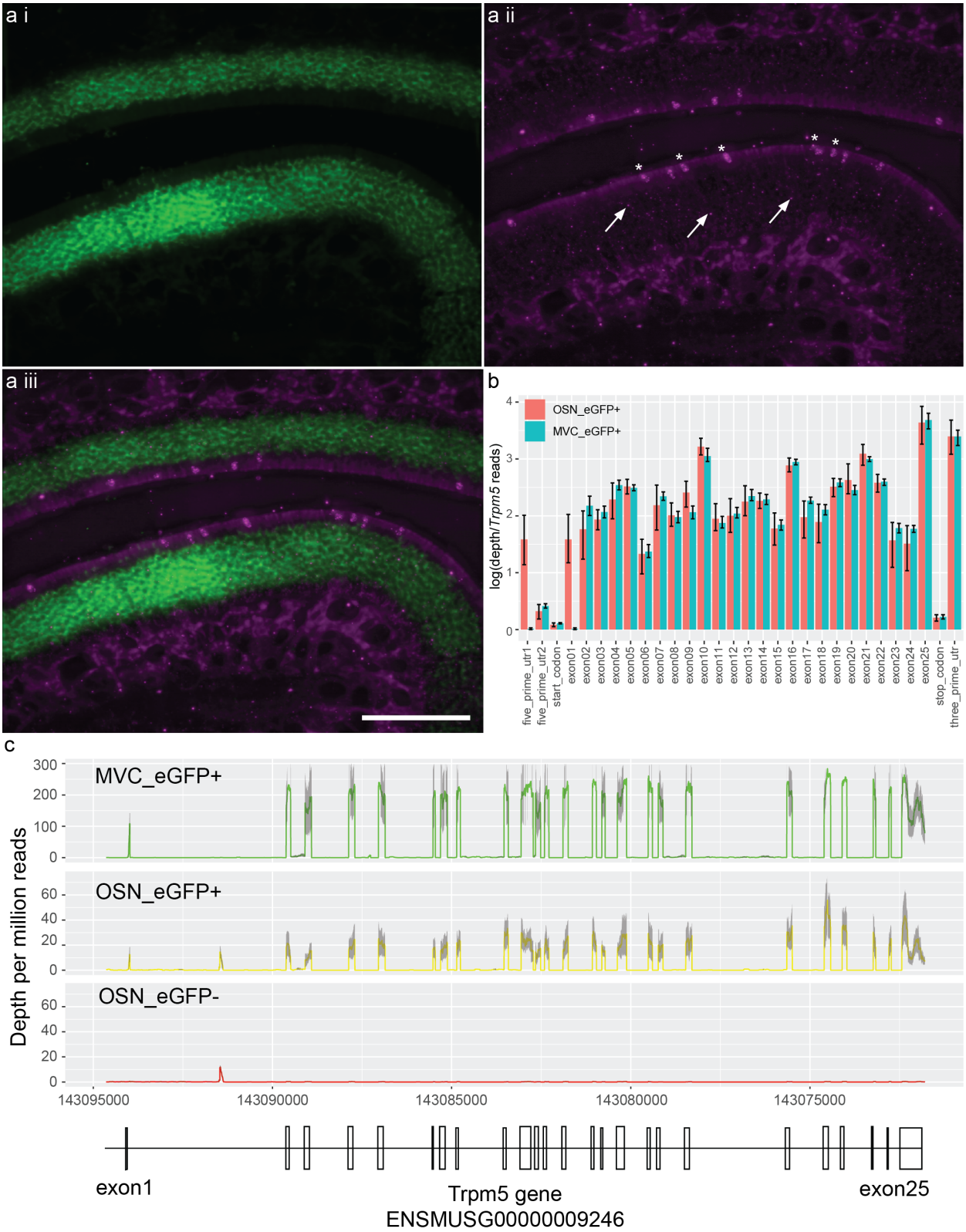
a i
a ii
a iii
b
OSN_eGFP+
MVC_eGFP+
log(depth/Trpm5 reads)
five_prime_utr1
five_prime_utr2
start_codon
exon01
exon02
exon03
exon04
exon05
exon06
exon07
exon08
exon09
exon10
exon11
exon12
exon13
exon14
exon15
exon16
exon17
exon18
exon19
exon20
exon21
exon22
exon23
exon24
exon25
stop_codon
three_prime_utr
c
MVC_eGFP+
OSN_eGFP+
OSN_eGFP-
Depth per million reads
143095000
143090000
143085000
143080000
143075000
exon1
Trpm5 gene
ENSMUSG00000009246
exon25

1135

1136 **Figure 3. Coverage of TRPM5 transcript by RNAseq in the different cell groups sorted**

1137 **from the olfactory epithelium**

1138 **a.** In situ for TRPM5 and OMP transcripts in the olfactory epithelium shows strong label for

1139 TRPM5 in MVCs (asterisks) and sparse labeling in the OSN nuclear layer (arrows). **i.** OMP, **ii.**

1140 TRPM5, **iii.** Composite. The scale bar is 100 μm.

1141 **b and c.** Coverage of the reads for the TRPM5 transcript for the different cell groups. Read

1142 coverage was computed with 'Samtools depth' over the region corresponding to the Trpm5 gene.

1143 **b.** Coverage per exon. All samples normalized to TRPM5 reads show distribution among exons

1144 with little difference between MVC and OSN_eGFP+ cells.

1145 **c.** Coverage shown per base pair as a function of location in the genomic DNA. Plots show read

1146 depth per base pair for each cell type normalized to total number of mapped reads. Gray shading

1147 indicates 95% confidence interval.

1148

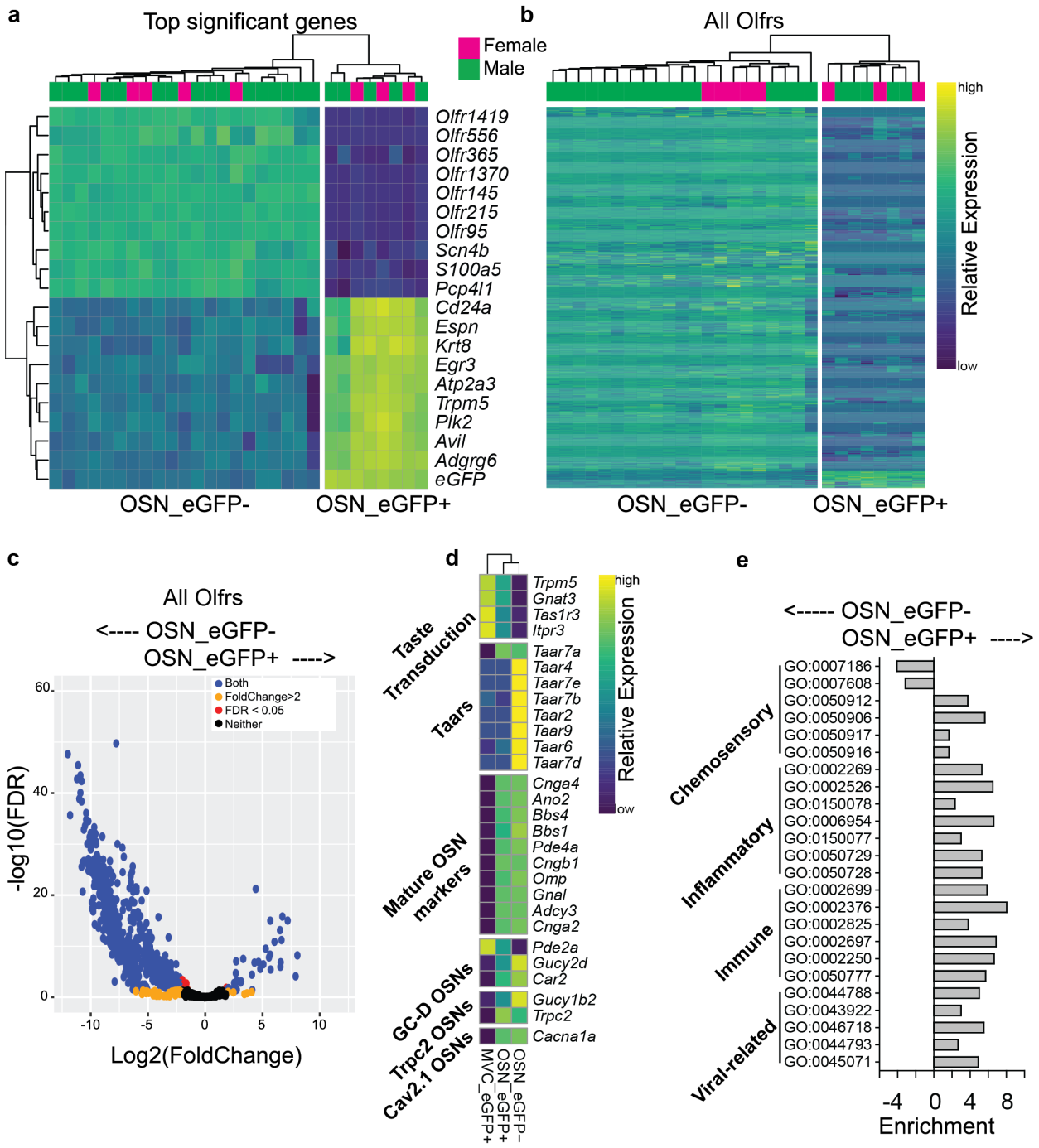

Figure 4. RNAseq comparison of OSN_eGFP- and OSN_eGFP+ cells.

a. Heatmap showing the top 10 upregulated and top 10 downregulated genes identified by DESeq2.

b. Heatmap showing all *Olfr* genes detected in the data.

1154 For both a and b, row and column order were determined automatically by the *pHeatmap*
1155 package in R. For each data point relative expression was calculated by subtracting the average
1156 row value from each individual value.
1157 **c.** Volcano plot of all Olfactory receptors, demonstrating the small number of enriched olfactory
1158 receptors in the OSN_eGFP+ population.
1159 **d.** Hierarchical clustering of transcripts for taste transduction and transcripts expressed in
1160 canonical and non-canonical OSNs identified by RNAseq as significantly different in expression
1161 between the cell groups. We compared expression of transcripts involved in taste transduction,
1162 canonical olfactory transduction, and non-canonical OSNs. The non-canonical OSNs considered
1163 here included guanilyl-cyclase D (GC-D) OSNs (Juilfs et al., 1997), Trpc2 OSNs (Omura and
1164 Mombaerts, 2014), Cav2.1 OSNs (Pyrski et al., 2018), and OSNs expressing trace amine-
1165 associated receptors (Taars) (Liberles, 2015). Transcripts identified by DESeq2.
1166 **e.** Gene ontology (GO) term enrichment was calculated from differentially expressed genes using
1167 *TopGO* in R. An enrichment value for genes with Fischer p value <0.05 was calculated by
1168 dividing the number of expressed genes within the GO term by the number expected genes (by
1169 random sampling, determined by *TopGO*).
1170
1171
1172

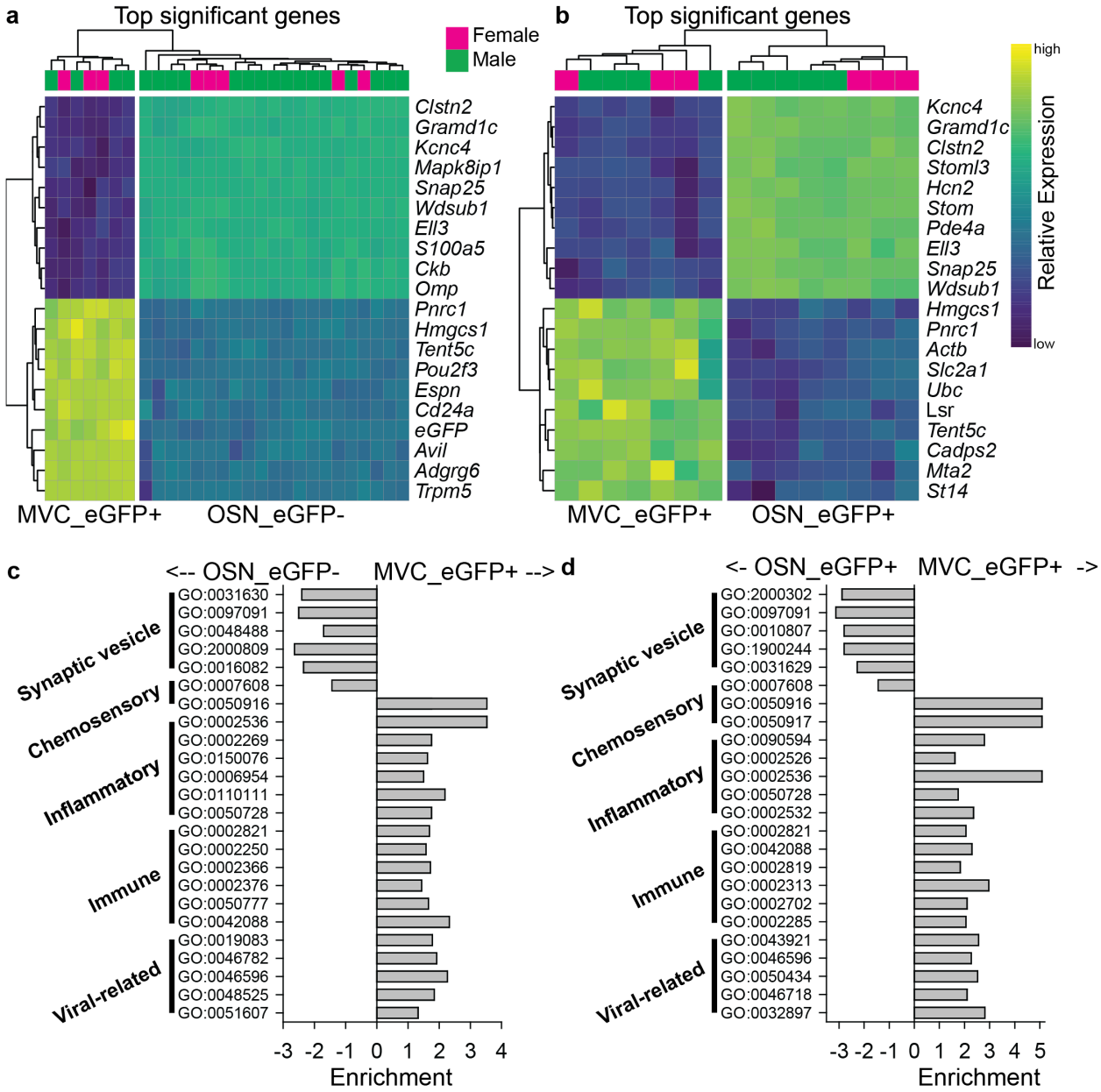

Figure 5. RNAseq comparison of OSN_eGFP- and OSN_eGFP+ vs. MVC_eGFP cells. **a and b.** Heatmaps showing hierarchical clustering of the top 10 upregulated and top 10 downregulated genes identified by DESeq2. **a.** OSN_eGFP- vs. MVC_eGFP cells. **b**. OSN_eGFP+ vs. MVC_eGFP cells. For both a and b, row and column order were determined automatically by the *pHeatmap* package in R. For each data point relative expression was calculated by subtracting the average row value from each individual value.

1180 **c and d.** Gene ontology (GO) term enrichment was calculated from differentially expressed

1181 genes using *TopGO* in R. **c.** OSN_eGFP- vs. MVC_eGFP cells. **d**. OSN_eGFP+ vs.

1182 MVC_eGFP cells. An enrichment value for genes with Fischer p value <0.05 was calculated by

1183 dividing the number of expressed genes within the GO term by the number expected genes (by

1184 random sampling, determined by *TopGO*).

1185

1186

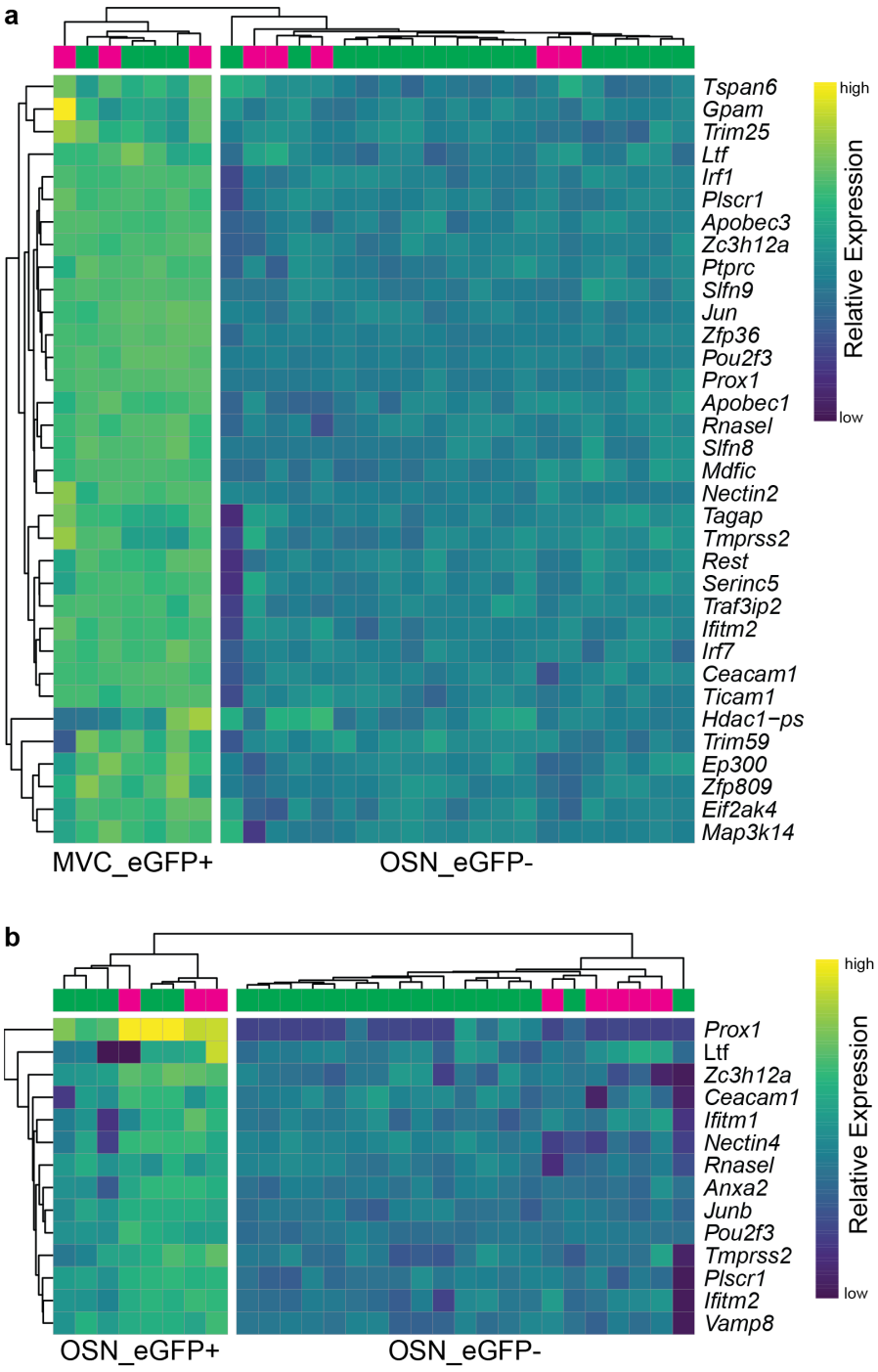

Figure 6. Significant differences in virally-related gene ontology. Heatmaps show hierarchical clustering of significantly differentially expressed genes identified by DESeq2. **a.** MVC_eGFP cells compared to OSN_eGFP-. **b.** OSN_eGFP+ compared to OSN_eGFP-.

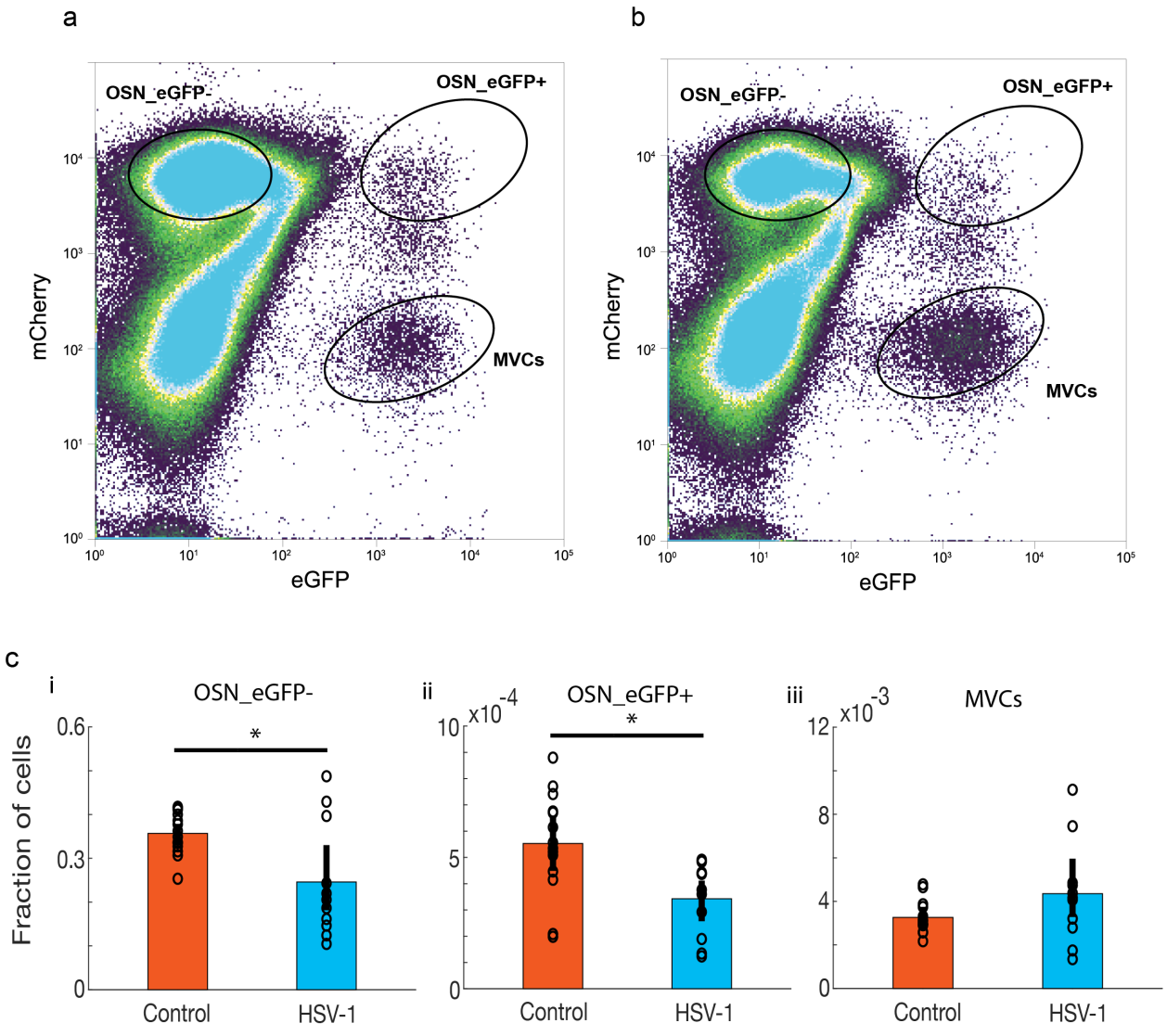

Figure 7. Intranasal inoculation with HSV-1 elicits a decrease in OSNs.

a and b. Distribution of mCherry and eGFP fluorescence intensity for FAC-sorted cells that either were not infected (**a**) or were inoculated intranasally with 10 µL of solution per naris (20 µL total with HSV-1 (1x 10^6 PFU/naris; McKrae strain) 5 DPI (**b**).

c. Fraction of total cells for OSN_eGFP- (**i**), OSN_eGFP+ (**ii**) or MVC (**iii**) cell groups. GLM analysis yielded significant effects for the fraction of OSN_eGFP- compared to MVCs ($p<0.001$) and for the interaction between the fraction of OSN_eGFP- compared to MVCs and HSV-1 treatment ($p<0.001$, 75 observations, 69 d.f., GLM F-statistic=111 and p-value < 0.001, n=14

1201 mice for control, n=11 mice for HSV-1 inoculation). Asterisks denote a significant difference

1202 post-hoc with t-test p-value < pFDR = 0.047.

1203

1204 **Supplemental Information**

1205

1206

1207 **Transcriptional profiling reveals TRPM5-expressing cells involved in viral infection in the**

1208 **olfactory epithelium**

1209

1210 B. Dnate' Baxter[1,2,‡], Eric D. Larson[3 ‡], Paul Feinstein[4], Arianna Gentile Polese[1,2], Andrew N.

1211 Bubak[5], Christy S. Niemeyer[5], Laetitia Merle[1,2], Doug Shepherd[6], Vijay R. Ramakrishnan[3],

1212 Maria A. Nagel[5], and Diego Restrepo[1,2,*]

1213

1214

1215 **Figure 4 – figure supplement 1. Excel worksheet with the results of comparison of gene**

1216 **transcription between OSN_EGFP+ and OSN_EGFP-.**

1217

1218 **Figure 4 – figure supplement 2. Metadata for the RNAseq.**

1219

1220 **Figure 5 - figure supplement 1. Excel worksheet with the results of comparison of gene**

1221 **transcription between MVC_eGFP cells and OSN_EGFP-.**

1222

1223 **Figure 5 - figure supplement 2. Excel worksheet with the results of comparison of gene**

1224 **transcription between MVC_eGFP cells and OSN_EGFP+.**

1225

1226

1227

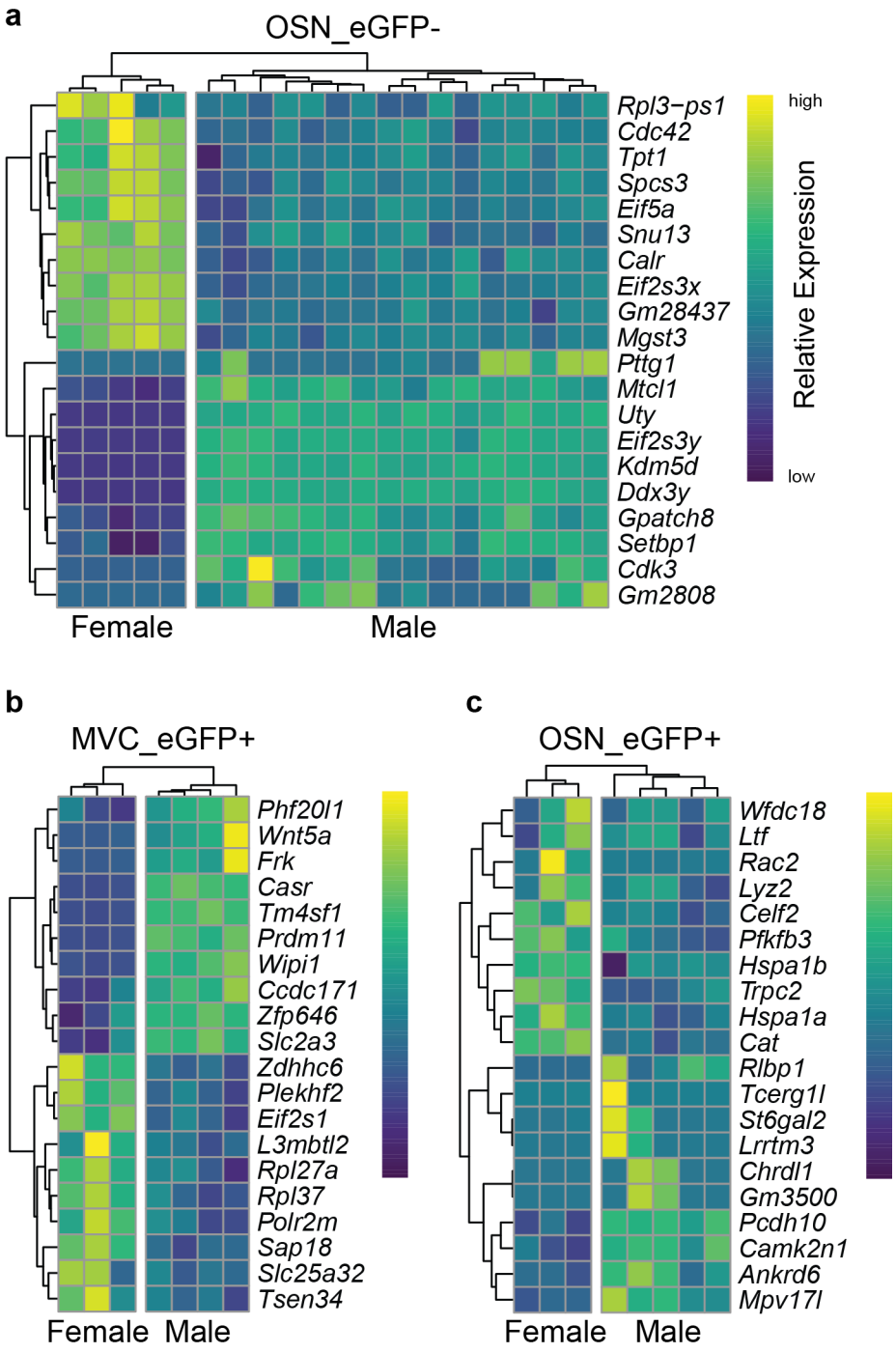

Figure 5 – figure supplement 3. Hierarchical clustering of transcripts identified by RNAseq as significantly differentially expressed between male and female. a. OSN_eGFP-. **b.** MVC_eGFP cells **c.** OSN_eGFP+. Transcripts identified by DESeq2.

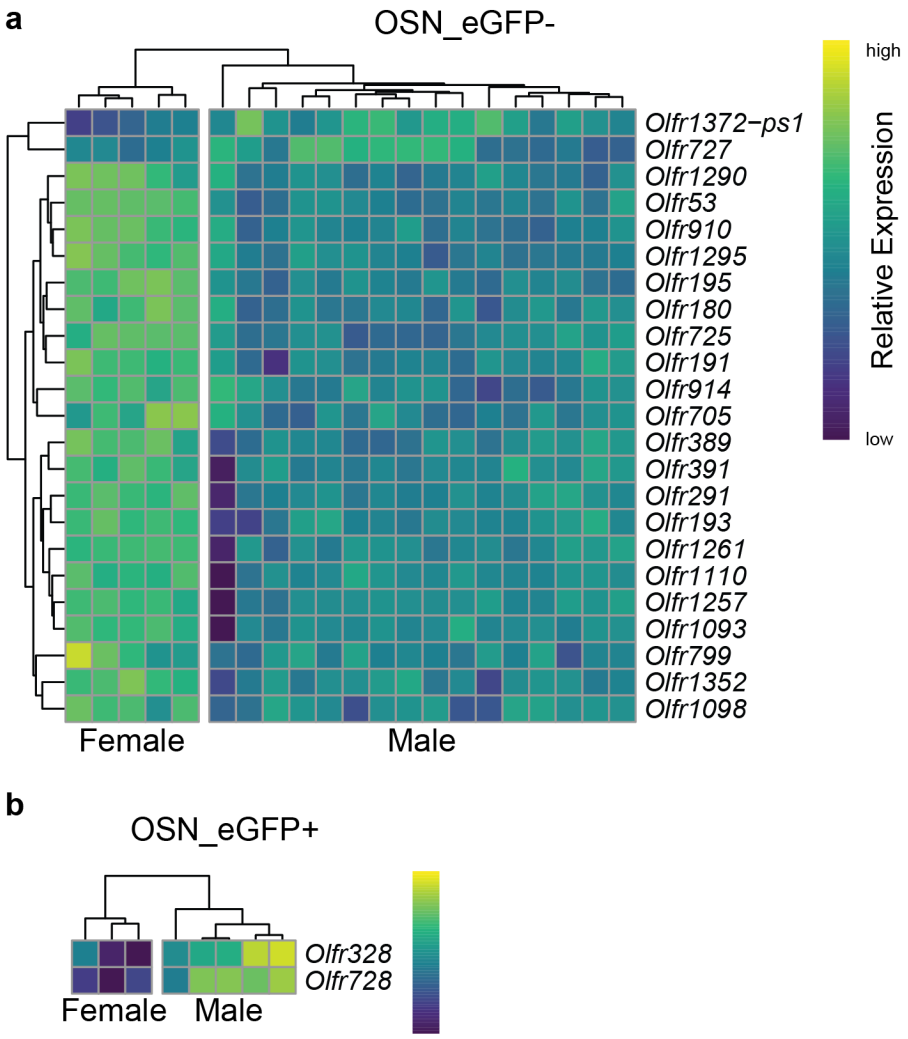

Figure 5 – figure supplement 4. Hierarchical clustering of olfactory receptor transcripts identified by RNAseq as significantly differentially expressed between male and female. a. OSN_eGFP-. **b.** OSN_eGFP+. Transcripts identified by DESeq2.

1238 **Figure 6 – figure supplement 1. Excel worksheet with the results of gene ontology**

1239 **enrichment analysis for OSN_eGFP+ compared to OSN_eGFP-.**

1240

1241 **Figure 6 - figure supplement 2. Excel worksheet with the results of gene ontology**

1242 **enrichment analysis for MVC_eGFP cells compared to OSN_EGFP-.**

1243

1244 **Figure 6- figure supplement 3. Excel worksheet with the results of gene ontology**

1245 **enrichment analysis for MVC_eGFP cells compared to OSN_EGFP+.**

1246

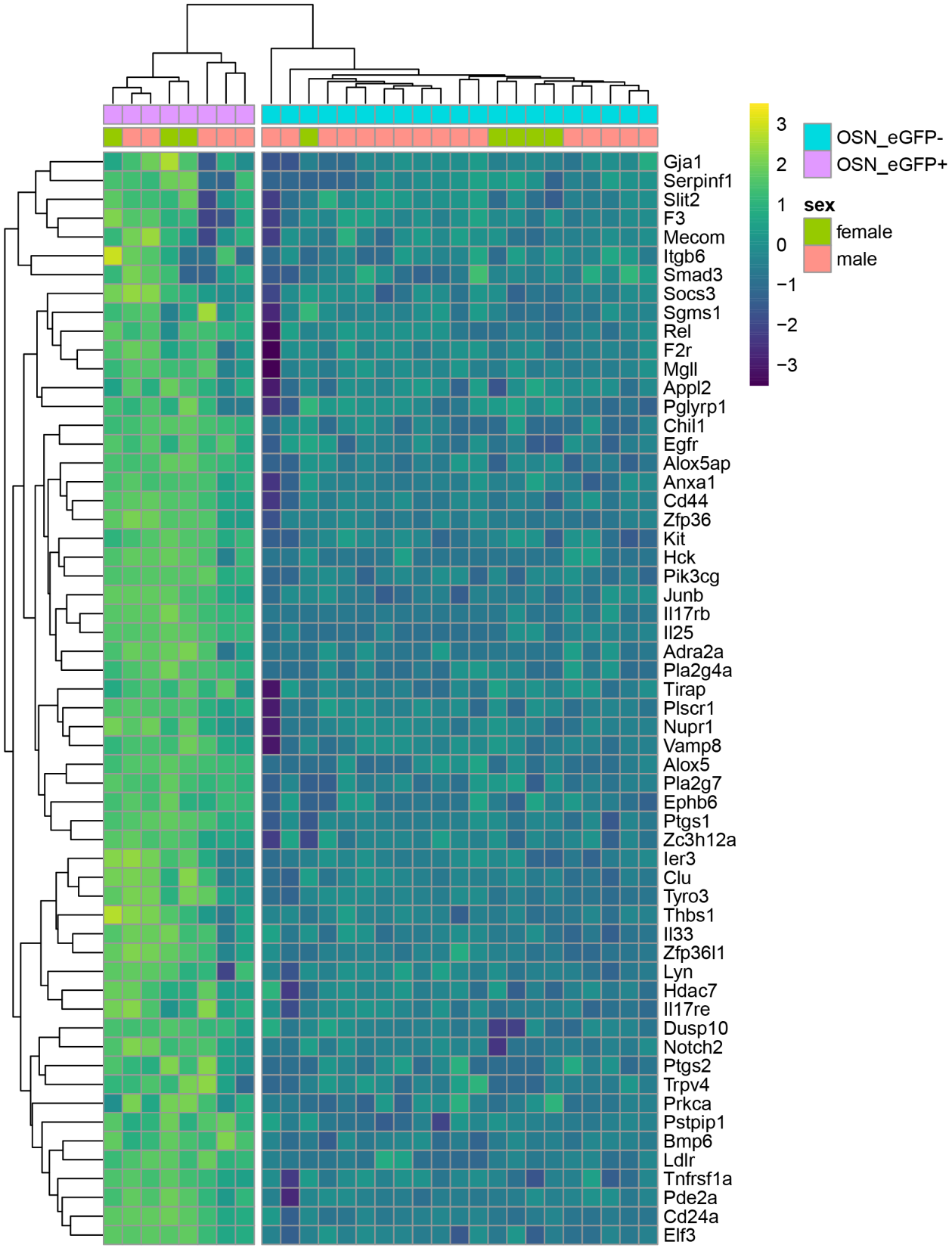
Gja1
Serpinf1
Slit2
F3
Mecom
Itgb6
Smad3
Socs3
Sgms1
Rel
F2r
Mgll
Appl2
Pglyrp1
Chil1
Egfr
Alox5ap
Anxa1
Cd44
Zfp36
Kit
Hck
Pik3cg
Junb
Il17rb
Il25
Adra2a
Pla2g4a
Tirap
Plscr1
Nupr1
Vamp8
Alox5
Pla2g7
Ephb6
Ptgs1
Zc3h12a
Ier3
Clu
Tyro3
Thbs1
Il33
Zfp36l1
Lyn
Hdac7
Il17re
Dusp10
Notch2
Ptgs2
Trpv4
Prkca
Pstpip1
Bmp6
Ldlr
Tnfrsf1a
Pde2a
Cd24a
Elf3
3
2
1
0
−1
−2
−3
OSN_eGFP-
OSN_eGFP+
sex
female
male

1247

1248 **Figure 6- figure supplement 4. Significant differences in inflammation gene ontology for**

1249 **OSN_eGFP+ compared to OSN_eGFP-.**

1250

OSN_eGFP-
MVC_eGFP+
sex
female
male
3
2
1
0
−1
−2
−3
Rell2
Zfp365
Lynx1
Rell1
Rora
Tcirg1
Gja1
Sgms1
Sulf1
Tnip2
Relt
Hdac7
Serpina3n
Nupr1
Mgll
Reg3g
F3
Pglyrp1
F2r
Tnfaip3
Tgfb2
Vamp8
Ccn3
Tirap
Plscr1
Rel
Itgav
Il17re
Mdk
Mif
Il1rap
Prcp
Adora1
Tnip1
Bcor
Itgb6
Gprc5b
Sall1
Pstpip1
Clu
Tnfrsf1a
Chst2
Gstp1
H2−T23
Smad3
Kit
Hck
Pik3cg
Pde2a
Cd24a
Lyn
Serpinf1
Anxa11
Il4ra
Ldlr
Zfp36l2
Elf3
Jun
Junb
Adra2a
Il17rb
Il25
Jund
Pdcd4
Pla2g4a
Appl2
Anxa1
Cd44
Zfp36
Ephb6
Nfkbiz
Ptgs1
Zc3h12a
Nr1d1
Ceacam1
Pla2g7
Thbs1
Adrb2
Chil1
Bmp7
Egfr
Socs3
Ticam1
Stat5a
Ptgs2
Nfkbia
Thrb
Mecom
Notch1
Slit2
Stap1
Ets1
Ier3
Prkca
Alox5
Zfp36l1
Trpv4
Alox5ap
Tyro3
Relb
Uaca
Parp4
Ano6
Sbno2
Dusp10
Notch2
Ndst1
Snap23

1251

1252 **Figure 6- figure supplement 5. Significant differences in inflammation gene ontology for**

1253 **MVC_eGFP+ compared to OSN_eGFP-.**

1254

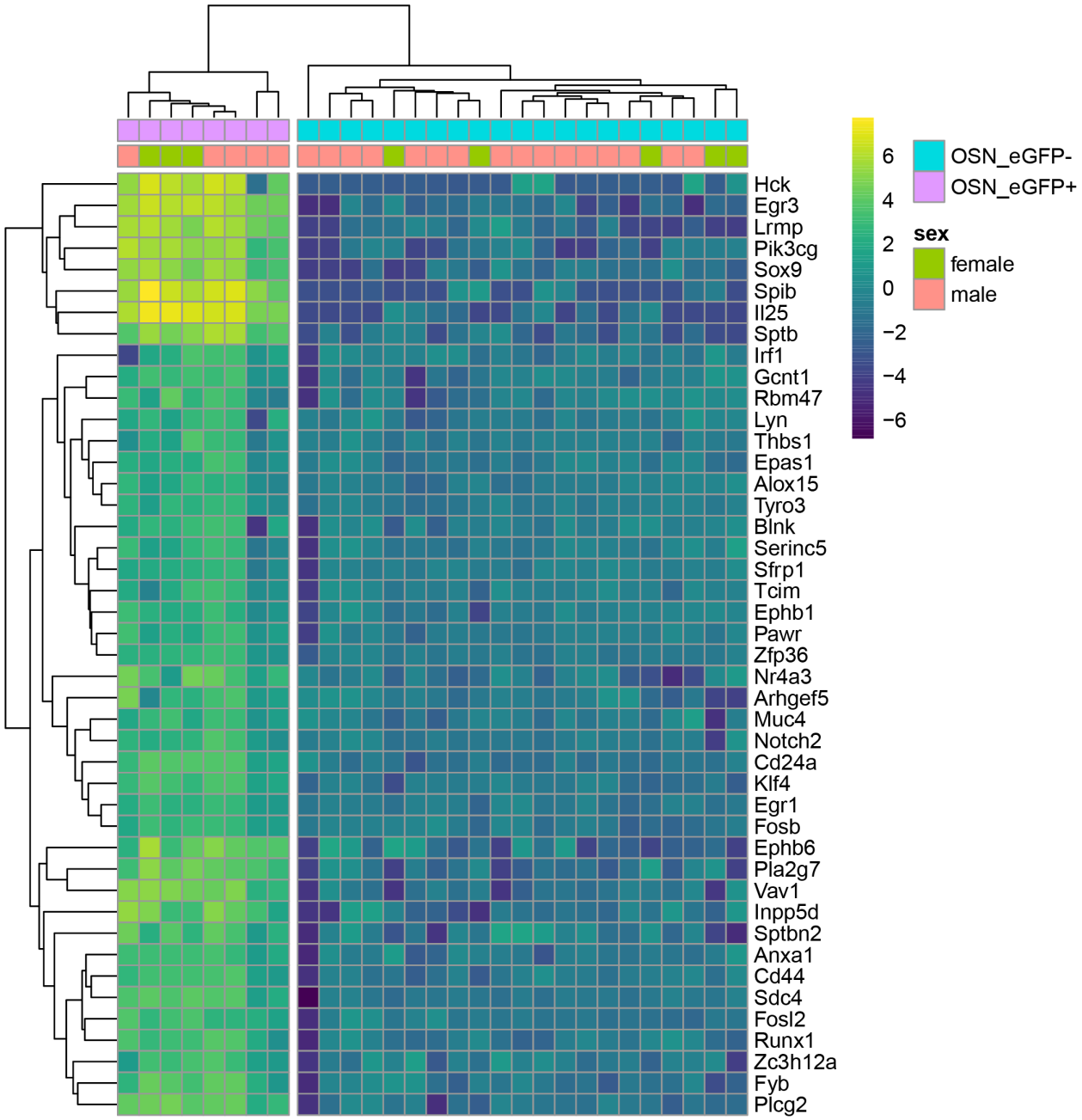

Figure 6- figure supplement 6. Significant differences in immune gene ontology for OSN_eGFP+ compared to OSN_eGFP-.

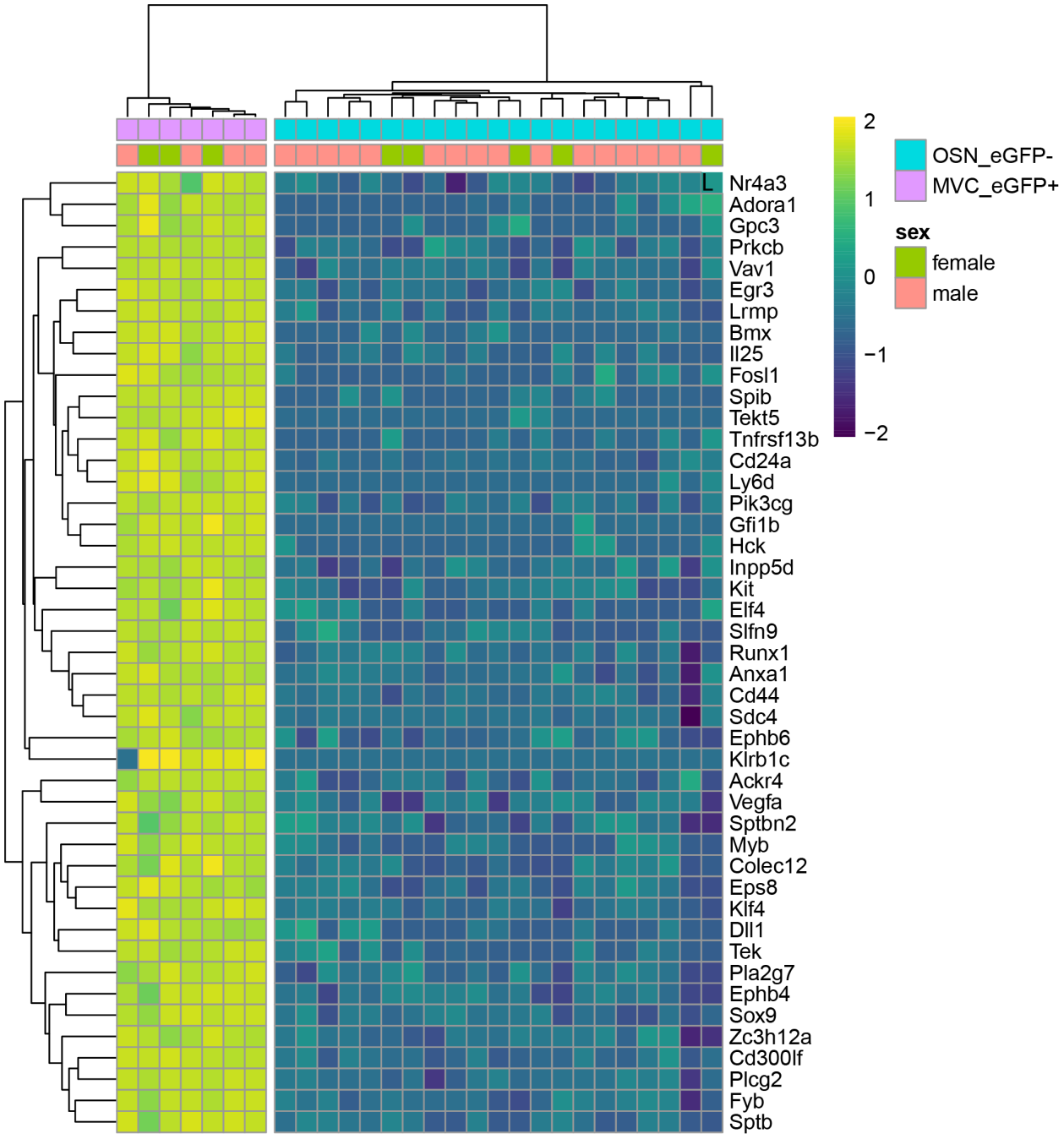

Figure 6- figure supplement 7. Significant differences in immune gene ontology for MVC_eGFP+ compared to OSN_eGFP-.